CONDITION MONITORING OF TAPER ROLLER BEARING

Narendiranath Babu T

1/29/2025

Publication Partner:
International Journal of Scientific and Research Publications (ISSN: 2250-3153)

CONDITION MONITORING OF TAPER ROLLER BEARING

Narendiranath Babu T

Publishing Partner:
IJSRP Inc.
www.ijsrp.org

ISSN 2250-3153
9 772250 315302

Preface

PREFACE is an introduction to a Monograph or other literary work written by the work's author. A preface is a section or page of the front and back matter of a book that includes explanatory remarks about the book.

The preface often closes with acknowledgements of those who assisted in the literary work.

Copyright and Trademarks

Publication Partner:
International Journal of Scientific and Research Publications (ISSN: 2250-3153)

Authors

Narendiranath Babu T
School of Mechanical Engineering
Vellore Institute of Technology, Vellore

TABLE OF CONTENTS

Abstract

In industries, bearing plays a crucial part in rotating machineries. Any fault in the bearing causes major breakdown of rotating machineries. Therefore, it becomes essential to develop a system that can detect and classify the faults in bearings in order to reduce downtime. The research involves an experimental investigation to diagnose and classify the faults with the help of frequency spectrum analysis and advanced signal processing techniques. The experiment involves the vibrational signal analysis on various faults in taper roller bearing. The classifications are characterized corresponding to four load conditions i.e. no load, 100gms, 200gms, 300g, and faulty bearing i.e. outer raceway defect, inner raceway defect and roller defect. Time domain features are reformed to frequency domain features followed by bi-orthogonal wavelet transform. A comparison study is shown between a Butterworth filter and bi-orthogonal wavelet transform to show the effectiveness of the latter method. Also, the efficiency of two neural network is compared using Confusion Matrix, where Artificial neural network is 95% efficient and deep neural network is 99% efficient. The research also shows the same experimentation for acoustic emissions. Where the fault classification using ANN got a efficiency of 96% and using DNN, the efficiency was 98%.

LIST OF TABLES

LIST OF FIGURES

LIST OF SYMBOLS AND ABBREVIATIONS

ANN	Artificial Neural Network
AC	Alternating Current
EDM	Electronical Discharge Machining
RBF	Radial Basis Function
rpm	Revolution per minute
MMDA	Matrix method of dimensional analysis
FFT	Fast Fourier Transform
Fs	Sampling Frequency
BPNN	Back propagation Neural Network
MLP	multilayer perceptron
PNN	Probabilistic Neural Network
NN	Neural Networks
EMD	Empirical mode decomposition
DNN	Deep neural network
BWT	Biorthogonal wavelet transform
FEM	Finite element analysis
Fc	Cut-off frequency
CNN	Convolutional neural network
KDA	Kernel discriminate analysis
EWT	Empirical wavelet transform
KECA	Kernel entropy component analysis
DAS	Data acquisition system
ROC	Receiver operating characteristics
BPOF	Ball pass outer race frequency
BPIF	Ball pass inner race frequency
BFS	Ball frequency for spin
FTF	Fundamental train frequency

CHAPTER 1

INTRODUCTION AND LITERATURE REVIEW

1.1 INTRODUCTION

Roller bearings are vital part of all rotating machines, their main function is to allow the rotational motion of the shaft with respect to a fixed support structure. During operation bearings have to endure large dynamic loadings produced in the machinery and transferred to bearing parts. Roller bearings in general tend to fail due to defects generated during operation. Taper roller bearings more importantly were designed to reduce friction and in turn reduce heat generated while in rotation. However even after the design advantage of tapered roller bearing which allows for even load transfer, bearings tend to fail due to various factors like "fatigue, wear, plastic deformation, corrosion, poor lubrication, faulty installation and incorrect design" as stated in review paper [Pankaj Gupta and M K Pradhan, 2016]. and explained by researchers [Sunnersjo C. S.1978, Wardle FP 1983 and Tallian 1965] in their respective works relating to bearings. Bearing failure causes production machinery to fail, in mass production industries failure can cost a lot in terms of meeting targets and reducing downtime as well as repair costs. Therefore, it becomes necessary to have a system that can detect, predict and classify bearing faults so that maintenance and replacement can be scheduled accordingly.

Most commonly to detect faults a method using FFT and extracted features from time domain are used to compare these include the Root mean square (RMS) value, wavelet energy change and energy of entropy mean. Initially a frequency domain plot is obtained using Fast Fourier transform (FFT) of the time domain signal which is then decomposed with the help of wavelets and ultimately the useful features are obtained and their variation is analysed for all conditions. It is noteworthy to realise that the extracted features of the vibration signal will show changes at characteristic frequencies when faults are present. Bearing faults are examined at various speeds and loads to collect vibration signal and various features (RMS, entropy mean, energy mean, etc.) are calculated and their variation is studied to classify fault types. [O.R. Seryasat *et al.* 2010]. However, this approach requires vibration domain expertise and the process cannot be made autonomous.

The general experiment involves these basic process, 1 Vibration and acoustic data acquisition using accelerometer and microphone sensor, 2 Signal processing to convert time domain signal to frequency-magnitude spectrum signal using FFT 3. Noise filtering using different methods such as STFT, orthogonal wavelet transforms, wavelet transform. 4. The use of the automated computational intelligence, artificial neural network and deep neural network, with iterative implementation of signal.

1.2 LITERATURE REVIEW

V. Hariharan, PSS Srinivasan **(2009)** conducted a study on vibration analysis of common roller bearings to classify faults induced in different locations using the time domain and frequency-magnitude spectrum statistical features. Two networks "RBFN" and "PNN" are used to identify the bearing abnormalities. The whole process of assessing 7 statistical parameters was written in MATLAB code. The parameters to be used include crest factor ratios and variant ratios as they are suitable for low shaft speeds while ratios of RMS values of signals are more suited for other shaft speeds.

P Shakya *et al.* **(2013)** work comprises of comparison between vibration from various identified parameters to defect fault for early seeded defects. The results of this work would be useful for the bearing fault diagnosis community in choosing appropriate vibration-based diagnostic parameters. There is a need to carry out further study at a lower defect size and a different defect topology (naturally occurring) to improve the reliability of the results.

Juan Xujuan *et al.* **(2014)** reviews the detailed study of taper roller bearings. The literature review is carried on design and analysis of taper roller bearings. The paper covers all techniques that have been developed for the purpose of design and engineering analysis of the bearing over a certain period of time. It mainly focuses on analysis of roller element bearings through "FEM" software technique. This paper does not deal with actual experimental study which can help validate techniques through experimental data.

Jaouher Ben Ali *et al.* **(2015)** show a method to differentiate between seven different bearing conditions depending on "Empirical mode decomposition (EMD)", mean of energy entropy and artificial neural network. Moreover to account for the time varying

patterns and characteristics of bearing vibration signal features are extracted based on "EMD energy entropy". A particular variable is formed which compares the features to predict the failure. Further their experimental results help in monitoring the bearing status and diagnose autonomously the seriousness of the defect accurately with the help of ANN without human intervention.

Oliver Janssens *et al.* **(2015)** uses "convolutional neural network" for the condition monitoring fault classification for an experimental setup and compares results with Frequency spectrum analysis techniques like kurtosis, crest factor and RMS value. It focuses on bearing fault diagnosis though three processes: data collection, useful feature extraction, and fault condition diagnosis. It establishes that convolutional neural networks work with better accuracy. They however do not compare other machine learning techniques such as PNN etc. Moreover, there is scope for testing the bearing under other kinds of induced defect conditions which were not explored.

Jamadar, Vakharia **(2016)** developed a mathematical model for relationship between Vibration characteristics and governing features using dimensional analysis methods and validating the model using experimental setup and readings. A Vibration response variable is taken as a function of various process parameters and final mathematical expression is obtained through MMDA technique. The paper shed light on dependence of vibration response on various process parameters however didn't talk about how vibration response would vary depending on type of defect for defect classification.

Hussein Al-Bugharbee, Irina Trendafilova **(2015)** worked on two stages signal pretreatments which is cleaning the noises into stationary linear spectrum and diagnosis using pattern recognition process. After fault identification for diagnosis, stages were set for severity estimation. To validate the methodology three cases are presented with different constraints on deep groove ball bearing.

Yassine Elyassami *et al.* **(2016)**, A slightly distinct approach taken by them aimed to determine and classify bearing faults using "Alfa stable" extraction and "Kernel Discriminate Analysis (KDA)" through experiment. The above states methods are developed to segregate the faults automatically. The method of neural networks-based machine learning is that it does not require manual input by professionals or advance

knowledge of the problem. The program is better at tasks where it is challenging to develop characterizing features, same cannot be said for the KDA based approach.

Pankaj Gupta, M. Pradhan **(2016)** implies study on various type of defects and sources of vibration present in machinery work. The paper mentions about various defects that arise in bearings while in operation as well as the causes vibration (variable compliance, geometrical imperfection, surface roughness, waviness, Raceway defect etc.). Further talks about various vibration response measurement approaches i.e. (time domain, frequency-magnitude spectrum).

Narendiranath Babu T. et al. **(2018)** compares the artificial neural network and deep neural network for defect analysis on Journal bearing. The signal processing was computed on initial 20% of the values for zero load condition of each faulty and healthy bearing. The paper proves DNN to be a better approach as the confusion Matrix summary estimates the efficiency of 100% compared to ANN's 98.5% efficiency rate. The DNN configures minor changes that are not recorded in ANN.

Jinglong Chen et al. **(2016)** study on generator bearing used in wind turbine. The extracted signal of faulty bearing was processed using "Empirical wavelet transform", which extracts modulated signal corresponding to fault induced. The study compared EWT with EMD and stablishes that EMT is more efficient tool for fault diagnosis. The EMT lacks to identify the fault feature for experimental bearing due to heavy external noises.

.Narendiranath Babu T. *et al.* **(2018)** study on self-aligning bearing using "Empirical mode decomposition (EMD)", which as described is a self adjusting signal processing tool which works on nonlinear and nonstationary data. Using cubic interpolation, maximum peak and minimum peak of the data are determined. Further, the paper highlights study about the comparison between ANN and DNN on six fault condition bearings. The available data was divided as 70% data is given to train, 15% for validation and remaining 15% to test the neural network.

Zhihai Wang et al. **(2016)** the study highlights the stages of features by analyzing signals on rolling bearing. The stages of features vary with sensitivity and weariness. It displays a method to absorb acoustic emission using a test rig. The de-noising tool uses wavelet packet transform and "kernel entropy component analysis (KECA)" Using

Gaussian kernel function to optimize on best kernel entropy component. A score graphs indicates the entropy weariness features. This method is easier and precise than previous processing methods.

Hosseini S. et al. **(2015)** the key highlight of the study is on lubrication situation throughout on journal bearing. The frequency identification and effective feature are de-noised using CWT and transform time signal for feature extraction of signal. The filtered data is work training the ANN, "Multi-layer Perceptron neural networks" and Genetic algorithm. The outputs are verified by "Raimondi and Boyd" charts.

1.3 KNOWLEDGE GAINED FROM THE LITERATURE

From Literature survey we can conclude that:

- Various types of defects and their cause were studied such as distributed defects, localized defects and sources of vibration like variable compliance and geometric imperfections.
- The study compared EWT with EMD and stablishes that EMT is more efficient tool for fault diagnosis. The EMT lacks to identify the fault feature for experimental bearing due to heavy external noises.
- It was established that neural network based techniques were more accurate and precise as compared to Frequency Spectrum Analysis.
- Neural Network works without human interaction and can be made fully autonomous.
- The paper highlights study about the comparison between ANN and DNN on six fault condition bearings. The available data was divided as 70% data is given to train, 15% for validation and remaining 15% to test the neural network.

1.4 GAPS IDENTIFIED

- Various other techniques involving PNN and other ANN have not been explored. Thus leaves area of doubt for better output performance. No judgement is made

on best of most optimized neural network. One must use either easily available or standardized software amongst all.

- The method of neural networks based machine learning is that it does not require human expertise or prior knowledge of the problem and is better in tasks where it is challenging to develop characterizing features, same cannot be said for the KDA based approach.
- The papers shed light on dependence of vibration response on various process parameters however didn't talk about how vibration response would vary depending on type of defect for defect classification.
- The software chosen show limit possibility. The papers do not compare other machine learning techniques such as PNN etc. Moreover there is scope for testing the bearing under other kinds of induced defect conditions which were not explored.

1.5 NEED FOR PRESENT RESEARCH

1. The researches have covered study on bearing, whereas the scope can be broadly involving all rotating systems that undergo wear and defect over time.
2. The involvement of neural network is easy but lengthy, hence a training algorithm with help if the data is directly classified without feature extraction.

CHAPTER 2

DESCRIPTION AND GOALS

2.1 OBJECTIVES

- Our aim is to develop a condition monitoring system that would successfully help detect and classify bearing faults with efficiency and accuracy relative to already existing systems.
- Create a suitable experimental setup that would resemble bearing running condition in operation with minimum external noise so it is easy to process vibration data.
- Acquire necessary equipment (accelerometers) and microphone as well as stable platform to record vibrations in all three axes and noise data.
- This would involve gaining knowledge of common bearing defects, gathering vibration and noise data and processing vibration and noise data so that it is suitable for use. Furthermore, understanding the functioning of various artificial neural networks and determining which would be best for our experiment with tapered roller bearings
- The signal processing phase would involve using appropriate filter for processing raw data. Next step would to apply FFT on the raw as well as filtered data.

2.2 SCOPE OF THE WORK

- A neural network-based condition monitoring system would help prevent excess downtime, reduced cost incurred due to machine repair and help prevent catastrophic failure of machinery therefore proving beneficial in the safety aspect. This is beneficial for mass production-based industries as reducing cost and increasing production are the main concerns. Further scheduling maintenance and allowing quick repair due to easier problem identification can be facilitated as well.
- The same approach of vibration data extraction and analysis with the help of neural networks can also be extended to other rotating machinery parts as well like gear boxes, turbine etc.

CHAPTER 3

TECHNICAL SPECIFICATIONS AND APPROACH

3.1 TECHNICAL SPECIFICATIONS

In order to design an appropriate condition monitoring system, it is essential to design a suitable experimental setup that should have a rotating bearing and be similar to bearing condition in actual operation. For experiment purposes a standard taper roller bearing was selected.

Bearing properties: SKF tapered roller bearing 30205 j2/q

Figure 1. 30205 j2/q Healthy Bearing

- Principal dimensions:

  Inside diameter d: 25mm

  Outside diameter D: 52mm

  Width T: 16.25mm

- Basic load ratings:

  Dynamic C: 30,8kN

  Static Co: 33,5kN

- Mass: 0,15kg

- Fatigue load limit Pu: 3.45kN

  Speed ratings:

  Reference speed: 10 000 r/min

  Limiting speed: 13 000 r/min

The setup was assembled and consisted of the following parts

- Fixed speed AC single phase induction motor: 0.66 hp, 1420 rpm
- Solid shaft: diameter 25mm
- Coupling: to connected the motor to the shaft
- Bearing casing: this was used to hold the bearing outer raceway in place
- Accelerometers: to record vibrations
- Fixed platform: platform to mount everything which is fixed to minimize internal vibrations.

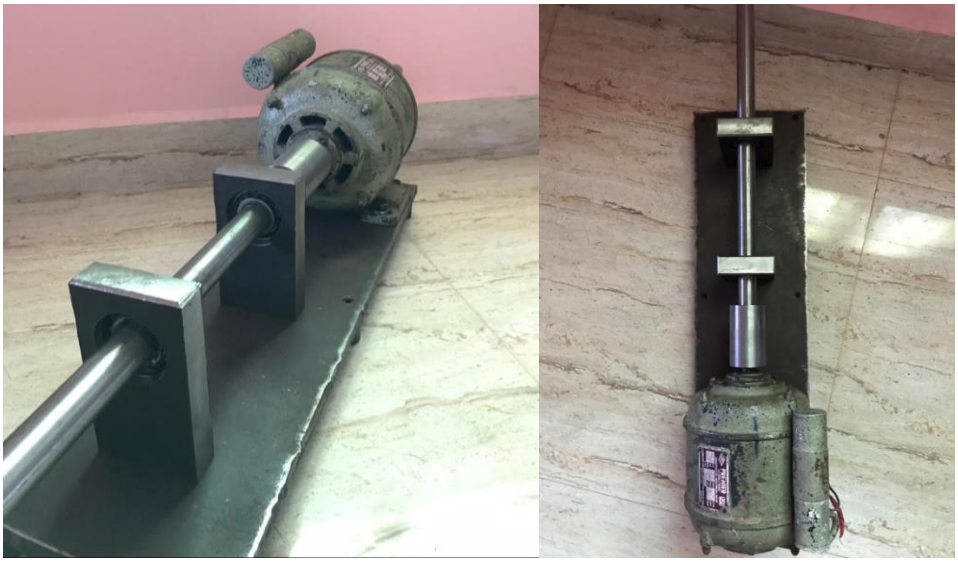

Figure 2. Assembled experimental setup

After setup completion common defects were induced into 4 test bearings for the experiment, these were:

- Outer raceway EDM cut depth 1mm.
- Inner raceway EDM cut, depth 1mm
- Impact on single roller with grinding wheel
- Impact on two rollers with grinding wheel

Figure 3. Different defects (a) Single roller defect (b) Outer race EDM cut (c) Double roller defect(d) Inner race EDM cut

EDM cuts were done using EDM wire cutting machine and the roller defects were induced using impact against a grinding wheel available in machine shop:

Figure 4. EDM wire cutting machine

The vibration and acoustic data of the taper roller bearing are collected using the setup in figure 1.

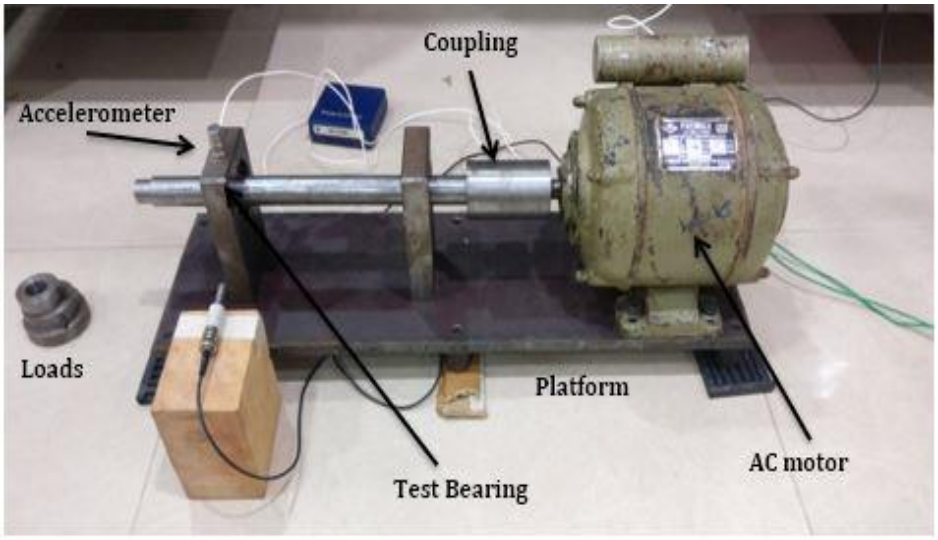

Figure 5. Experimental setup along with sensor mounted

The setup consists of fixed speed AC single phase induction motor with .66 hp and motor speed of 1420 rpm at no load condition. The Solid shaft of dia. 25mm is fixed to the AC motor via Coupling on one side. Two bearing casing are used to hold the bearing through the experiment. Four small circlips are used two placed bearings and two bearing to stabilize outer race of bearings. The other side of the shaft is reduced to 20mmto attach any load conditions. The bearings are deliberate impacted with the same faults as occurred in the industry. The bearings are induced with five bearing fault conditions namely as in figure 2. The faults are induced on the bearing with EDM cut of depth 1mm on Outer and Inner raceway of bearing. Two bearing are induced with single and double roller defect through grinding wheel.

To record the vibration data 8702/4B50 type accelerometers is used with specification - acceleration range of ± 50g, with transverse sensitivity of ± 5% and relative sensitivity of 100 mV/g. A four-channel data acquisition system (DAS) collects the vibration signal on taper roller bearing. The system reads maximum voltage of ± 5V with the sampling rate limit of 51.2 kb/s per channel. The DAS reads the vibration data of taper roller bearing through DEWESoft software. The software plots a graph between the

amplitude of the vibration(m^2/s) versus time period(s). The data readings are recorded in 20 seconds and 30 seconds time period. Using the MATLAB software, the complete time period of 50 second is analyzed and a 10 seconds data is collected where maximum noise is observed for respective faults. This time domain data is converted to frequency-magnitude spectrum data using FFT. Then, the signal generated are further processed to filter out the characteristic frequency of the system. A general flow of the procedure can be seen in fig. 3 to understand the working of the complete process.

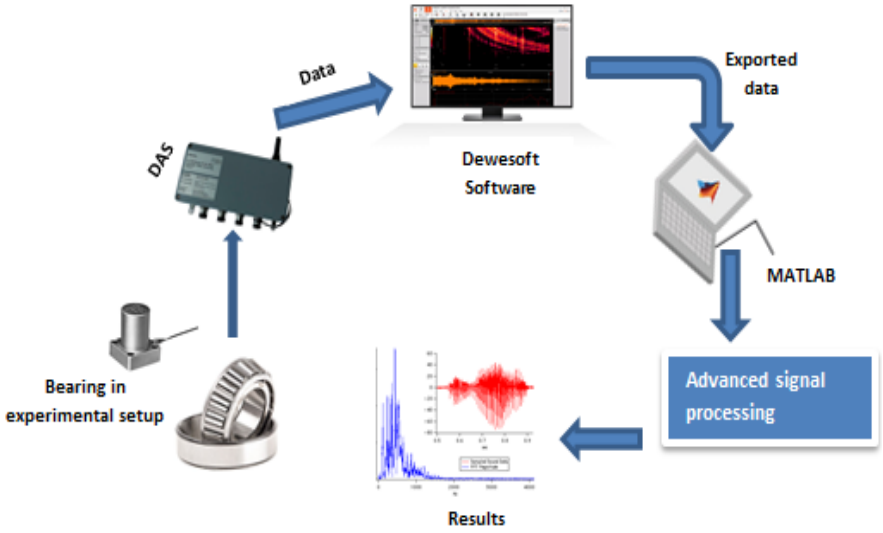

Figure 6. Condition monitoring system

CHAPTER 4

DESIGN APPROACH AND DETAILS

4.1 METHODOLOGY

The signal processing phase can be explained through the following flow chart

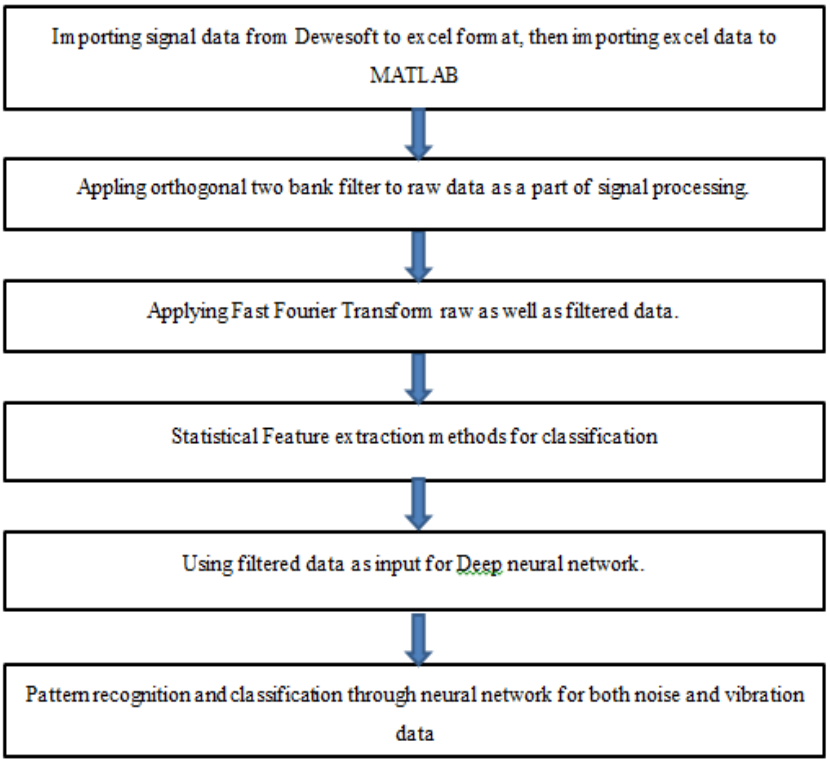

Figure 7. Signal processing flow chart

The characteristic frequencies cannot be distinguished from the frequency-magnitude spectrum of the raw signal because of the machine noise and many other factors. Therefore, it becomes essential to adopt precise signal processing methods to extract the characteristic bearing frequency components and their harmonics. Filters are

commonly used to de-noise the signal. However even filters tend to become ineffective at times where patterns vary with time. Wavelet transforms have proved very effective in identifying such features compared to standard FFT representation which is limited to stationary signals only. A comparison study of Butterworth and biorthogonal wavelet transform (Bior spline wavelets) is conducted on our data to validate the same. A flow chart explaining condition-based monitoring and fault detection using wavelet transforms is illustrated below in Figure 4.

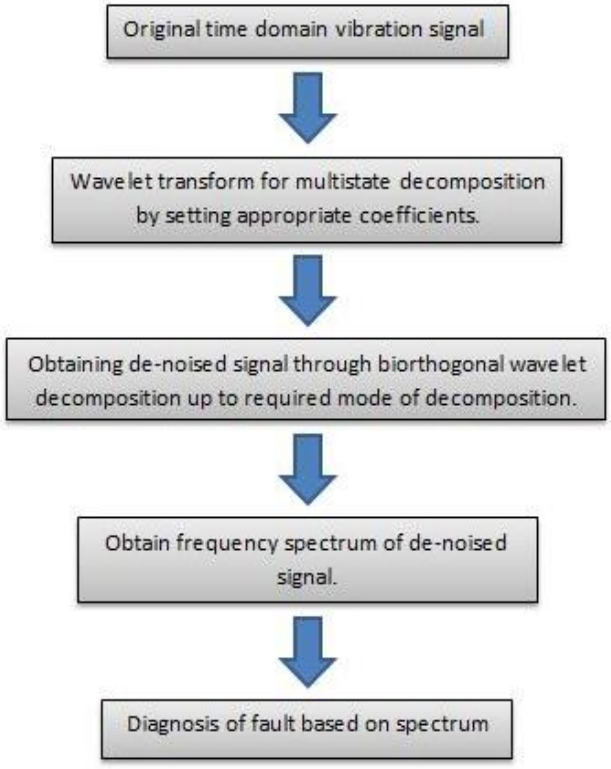

Figure 8. Work flow diagram of wavelet transform

4.1.1 Butterworth filter

The Butterworth filter is characterised as maximally flat amplitude response filter that is, there is no pass band ripple like in chebychev and elliptic filters. The Butterworth filters works on periodically changing function ω with respect to magnitude, as compared to other filters. The phase response plot of the filter varies with transfer function, 2N-1, and becomes nonlinear as the value of is raised. The filter consists of two parameters: cut-off frequency, sampling frequency and filter order when it is implemented in

MATLAB. The cut-off frequency varies from $\omega_0 = 1$ to $\omega_0 = 5$. The frequency magnitude response of the Butterworth filter is tending to flat in the passbands and downside until approaches 0 in the stopband.

$$G^2(\omega) = |H(j\omega)^2| = \frac{G_0^2}{1+\left(\frac{j\omega}{\omega_c}\right)^2} \quad (1)$$

The above equation illustrates the transfer function of filter where ω is the angular frequency in radians/s, j is the highest pass band gain and ω_c is the cut-off frequency. G_o is the DC at zero frequency (gain). The filter was formulated by British physicist Stephen Butterworth, he also showed that certain changes and modifications can be made to give low pass, high pass, band stop and band pass filters. The below plot in fig5 shows that the filter moves off towards zero in the area of the stop band.

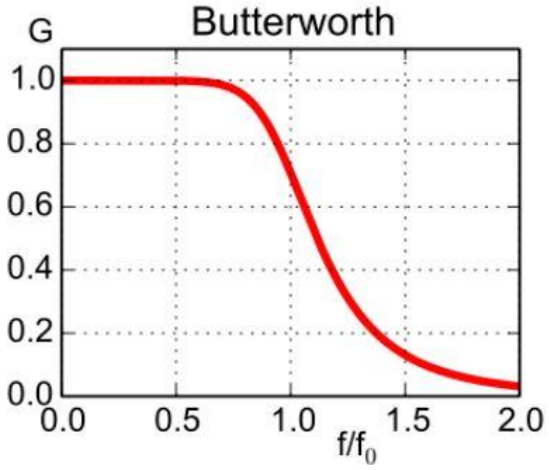

Figure 9. Frequency response of Butterworth filter

In signal processing step involved with this study the Butterworth filter was designed with the help of MATLAB's signal processing toolbox. As the vibration data required to use a low pass Butterworth filter parameter such as cut-off frequency and filter order were set by observing the FFT plot of the original signal. Band pass and band stop filters based on Butterworth design were also formulated in order to extract useful signal from the data.

4.1.2 Bi-orthogonal Wavelet Transform (BWT)

The BWT is invertible and different from orthogonal wavelet. The biorthogonal wavelet has one advantage of one degree of freedom over orthogonal wavelet. This allows biorthogonal wavelet transform to construct a symmetric wavelet function that eliminate

coefficient expansion. This symmetry of filter coefficient produces a linear phase transfer function. The wavelet transform helps in reducing the unwanted data and function into frequency components. This data is studied is scaled to matching resolution.

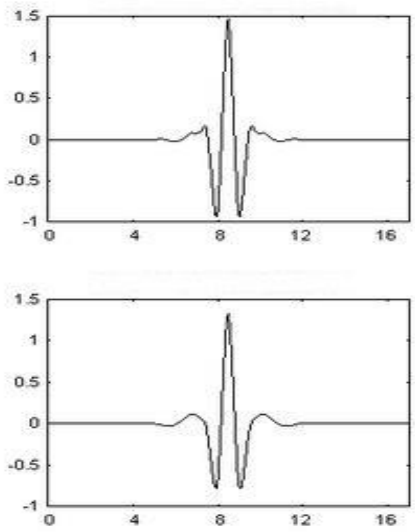

Figure 10. Biorthogonal wavelet

The biorthogonal wavelet transform consists of 2 scaling and 2 wavelet functions. These functions have multiscale approximation analyses which alters the coefficients. The biorthogonal condition to be satisfied for scaling through the given formula. (2)

$$\frac{1}{\sqrt{2}}\varphi\left(\frac{t}{2}\right) = \sum_{n=-\infty}^{+\infty} g[n]\phi(t-n)$$

The wavelet decomposition converts the signals into a low pass filter and a high pass filter. These filters are denoted in form of vectors as namely- Approximate Coefficients (cA1) and Detailed Coefficients (cD1). The wavelet removes the noise by compressing or suppressing the components of detailed coefficients which are made of high frequency noise and characteristic information of the machine fault. The exercised signals and approximate coefficients refabricate the original signal by using multiple iteration, hereby making the signal noise free.

4.1.3 Artificial Neural Network (ANN)

The vibration signal data of five conditions on taper roller bearing for 50 seconds is collected. While analyzing the data, 10 seconds data is processed for de- noising. Initially, the time domain data of each condition is calculated for the time domain features. The time domain features include ten features i.e. root mean square (RMS), Kurtosis factor, Skewness, Peak to Peak, Crest factor, Shape factor and Impulse factor (IF), Standard deviation, Margin factor (MF), total energy(E).

(3)

(4)

$$RMS = (\frac{1}{N}\sum_{i=1}^{N} x_i^2)^{1/2}$$

(5)

$$Kurtosis = \frac{1}{N}\sum_{i=1}^{N} \frac{(x_i - \bar{x})^4}{\sigma^4}$$

(6)

(7)

$$Skewness = \frac{1}{N}\sum_{i=1}^{N} \frac{(x_i - \bar{x})^3}{\sigma^3}$$

(8)

$$Peak\ to\ Peak = x_{max} - x_{min}$$

$$Crest\ Factor = \frac{max|x_i|}{RMS}$$

(9)

$$Shape\ Factor = \frac{RMS}{\frac{1}{N}\sum_{i=1}^{N}|x_i|}$$

(10)

$$Impulse\ Factor = \frac{max|x_i|}{\frac{1}{N}\sum_{i=1}^{N}|x_i|}$$

(11)

$$Margin\ Factor = \frac{max|x_i|}{(\frac{1}{N}\sum_{i=1}^{N}|x_i|^{\frac{1}{2}})^2}$$

(12)

$$Standard\ deviation = \sqrt{(\frac{1}{N-1}\sum_{i-1}^{N} x - \bar{x}^2)}$$

$$Total\ energy = \sum_{i=1}^{N} E_i$$

From these features, a 10*100 matrix is formed, where each condition corresponds to 20 samples. These features access the bearing performance degradation over time. The

program can easily be validated through these features as the increase in degradation implies increase in magnitude over the time. the matrix formed is set as input and trained using pattern recognition tool in MATLAB. The available data is subdivided into training, testing and validation as 70% data is given to train, 15% for validation and remaining 15% to test the neural network. The neural network displays 5 outputs i.e. Performance plot, training plot, error histogram, receiver operating characteristics plot (ROC) and confusion matrix. The performance of the neural network is analyzed by cross entropy technique.

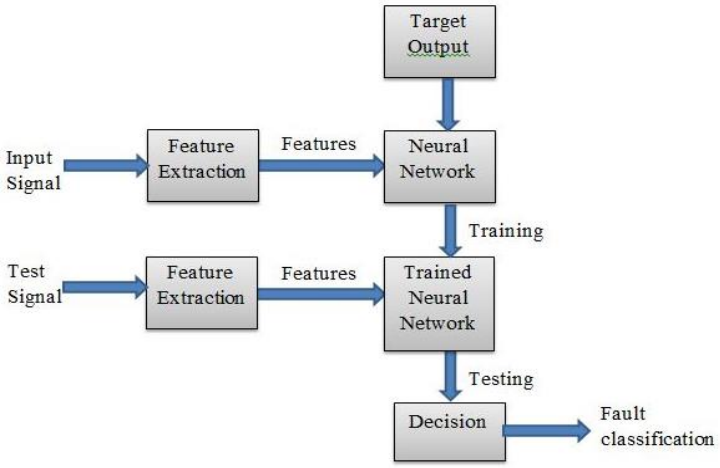

Figure 11. Work flow of Neural network

4.1.4 Deep Neural Network (DNN)

Deep neural network is basically a neural network that contains two or more networks. The basic procedure involves a learning rule which helps train the deep neural network after witch a specific input data would give output through the neural network. The multiple layers or the hidden layers are trained through back propagation algorithm. In this training function the errors are passed to previous middle layers to improve the network as implied by the name of the algorithm. Rectified linear unit function is used as an activator function. The same features are used to train DNN as well. These features are first extracted in the hidden layer through consecutive two layers of autoencoder. Then the features are used to train SoftMax layer for classification of the faults. The basic architecture of the deep neural network can be shown in fig. 8.

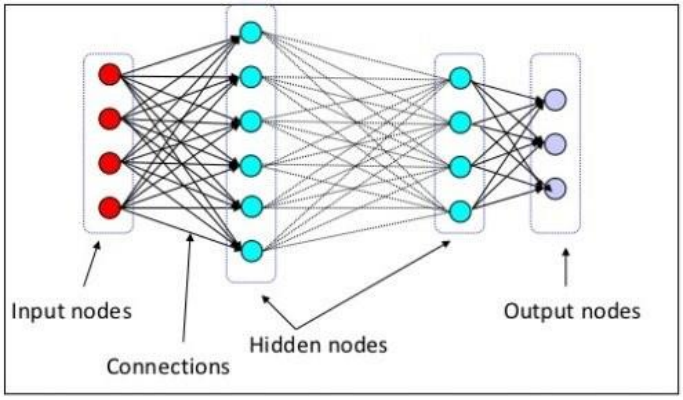

Figure 12. Deep Neural Network flow diagram

CHAPTER 5

MILESTONES

This work was divided in four stages to be completed in following order: -

- Literature Review
- Experimental Setup design and assembly
- Collecting reading for all experimental cases
- Advance signal processing and data validation
- Training neural network for classification

The Gantt chart highlights the milestone achieved over the period of 16 weeks.

CHAPTER 6

RESULTS AND DISCUSSION

6.1 Demonstration of Outputs

6.1.1 Collection of characteristic frequency of bearing conditions

To calculate the characteristic frequency of the vibration the equations formulated by T. A. Harris(1991) can be used –

Table 1. Characteristic frequency and calculated value

Characteristic frequency	Equation	Calculated Value
Shaft rotational frequency (Fs)	Shaft speed/60	23.67 Hz
Ball passing outer race frequency (BPOF)	$BPOF = Fs\frac{N_b}{2}(1-\frac{B_d}{P_d}cos\phi)$	170.97 Hz
Ball passing inner race frequency (BPIF)	$BPIF = Fs\frac{N_b}{2}(1+\frac{B_d}{P_d}cos\phi)$	231.42 Hz
Fundamental train frequency (FTF)	$FTF = \frac{Fs}{2}(1-\frac{B_d}{P_d}cos\phi)$	10.06 Hz
Ball frequency for Spin (BFS)	$BFS = Fs\frac{P_d}{2B_d}(1-\frac{B_d^2}{P_d^2}cos\phi)$	74.38 Hz

Where N_b is the number of rollers, B_d is the ball dia., P_d is the pitch dia. and ϕ is the contact angle of roller (^{o}).

Shaft speed= 1420 rpm ; N_b= 17 ; B_d= 5.91mm ; P_d= 38mm ; ϕ= 15^o

6.1.2 Validation of Healthy bearing vibration data

The vibration data of healthy bearing collected through the experimental setup is first validated to verify whether the setup is suitable for taking vibration readings and there is no excess of experimental noise. The original time domain vibration response of the healthy bearing is displayed in fig. 9. The useful features are hidden behind external noise and therefore need to be extracted. Frequency-magnitude spectrum of the original signal is laid out in fig. 10, also the extracted modes of the signal through biorthogonal wavelet transform are displayed in fig. 11. The corresponding frequency domain plot of the final decomposed signal is represented in fig. 12 and the peak amplitude of 0.043209 m^2/s is observed at 24.908 Hz which corresponds with the calculated natural frequency of vibration of the bearing. The Denoised signal is obtained through MATLAB's wavelet designer toolbox which involves wavelet decomposition, thresholding and signal reconstruction. In decomposition, the original signals with experimental disturbances are decomposed to 8 stages using BWT. In order to analyze the efficiency of wavelet transform, the output is compared with a commonly used low pass Butterworth filter output. Fig.10 shows a filtered signal where a low pass Butterworth filter has been used with appropriate cut off frequency. The comparison of the frequency spectrum of the two processed signals i.e. wavelet decomposed and filter show the superiority of the wavelet transform method as it is able to capture more than one component of characteristic frequency(harmonics).

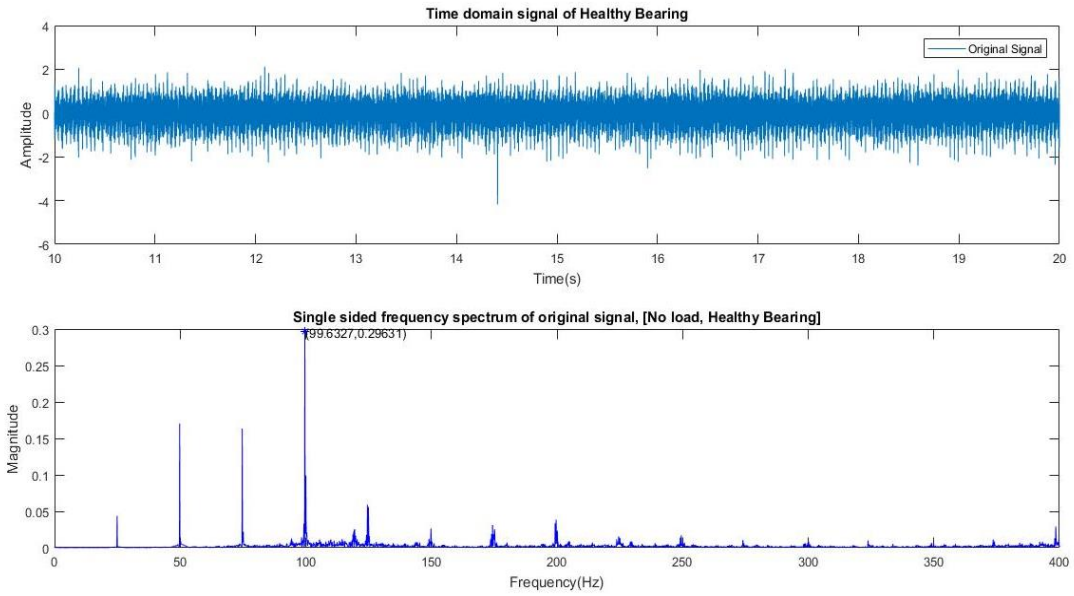

Figure 14. Time domain and FFT graph plot of healthy bearing

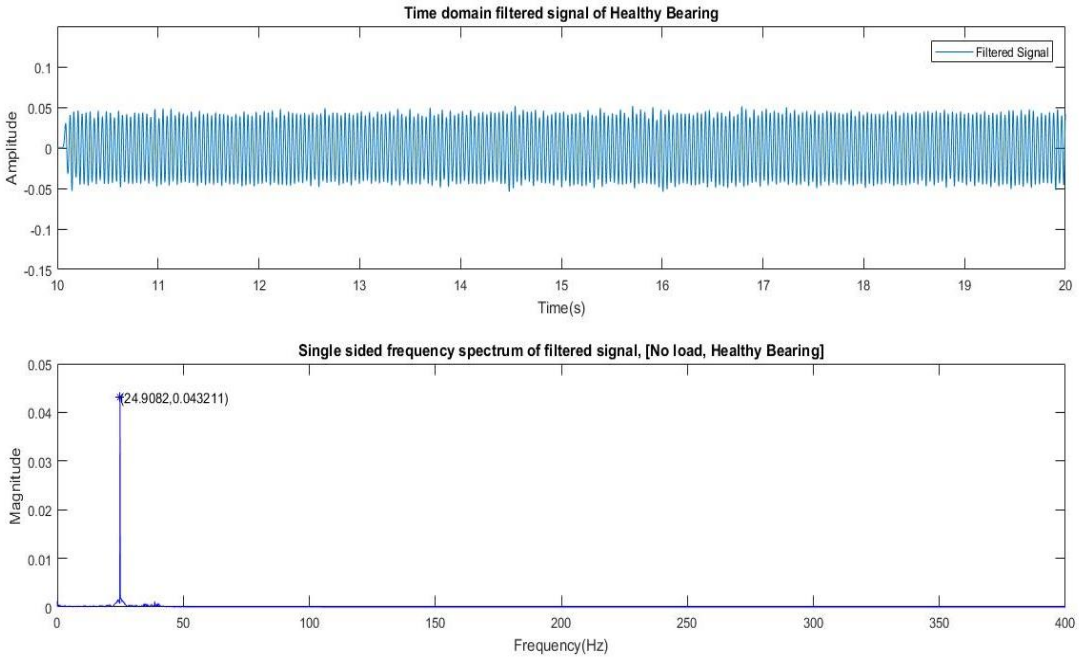

Figure 15. Butterworth filter of healthy bearing

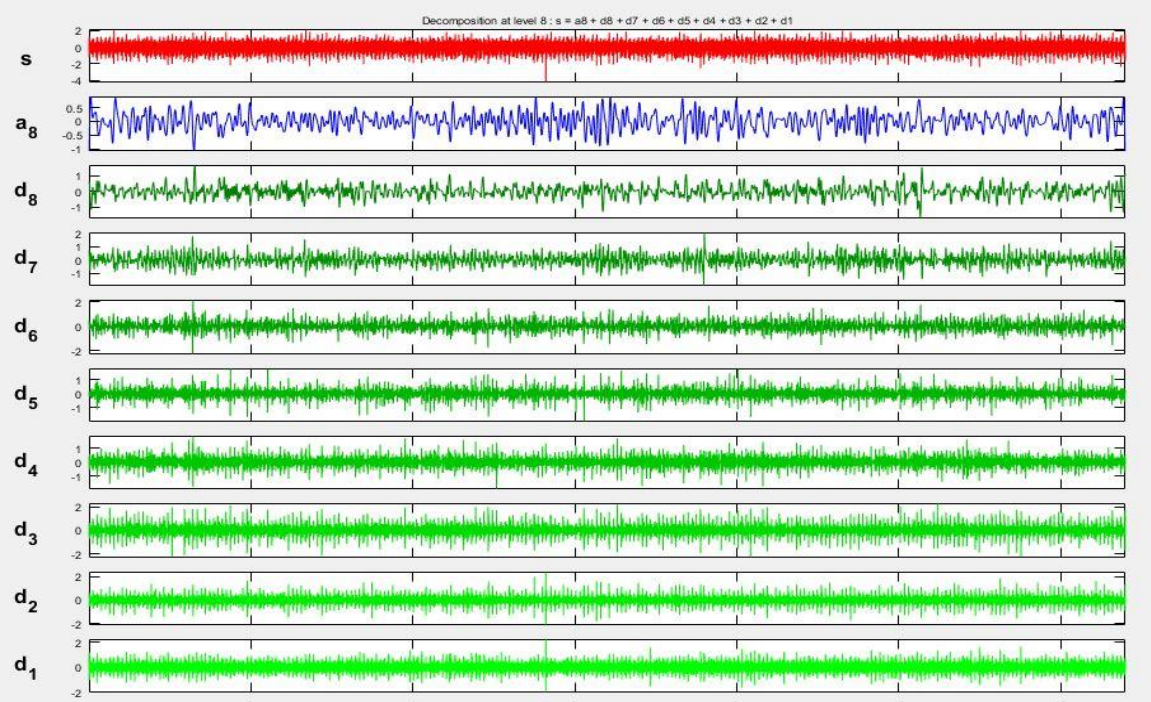

Figure 16. Wavelet decomposition of healthy bearing

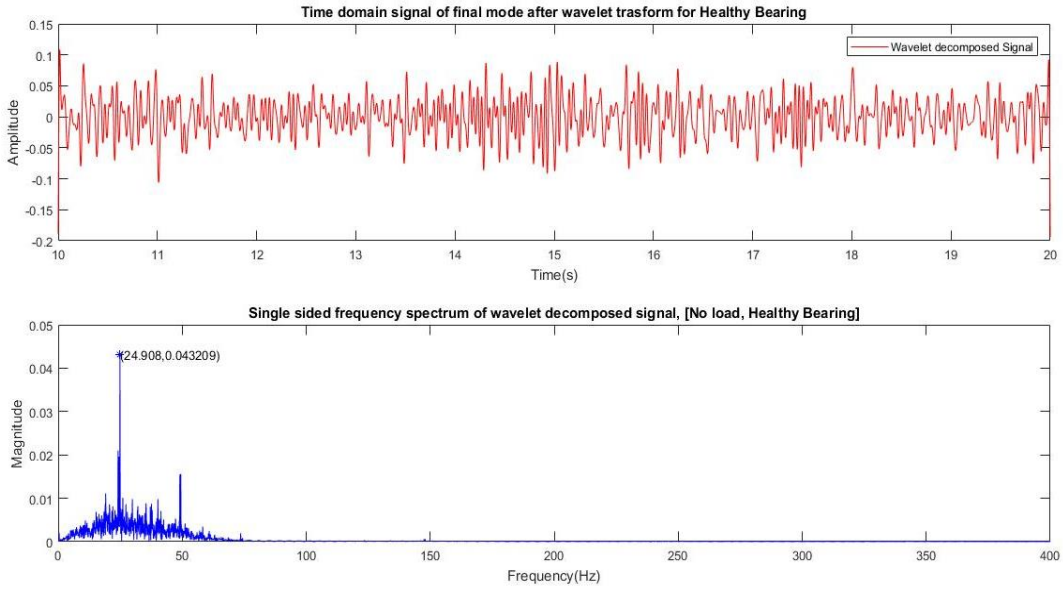

Figure 17. Wavelet decomposed time domain and FFT graph plot of processed of healthy bearing

6.1.3 Fault condition 1- Single Roller defect

The fault is induced on a single roller bearing by subjecting the healthy bearing through stone grinding wheel. The data of faulty bearing can be observed. The time domain vibration signal and its frequency spectrum are displayed in fig. 13. The butterworth filter as in fig. 14, is used to compare the amount of denoising with wavelet transform. The wavelet decomposed modes are highlighted in fig. 15 and the de-noised signal as well as its frequency spectrum are revealed in fig. 16. The peak amplitude after 5 modes of decomposition is observed at frequency of 74.9199 Hz as show in fig. 16 corresponds with BFS of the bearing and therefore indicates presence of defect on roller. Moreover, the peak amplitude is observed at BFS at relatively less modes of decomposition indicating that the impulses generated by the roller defect are significant compared to other noises involved in the experimental setup.

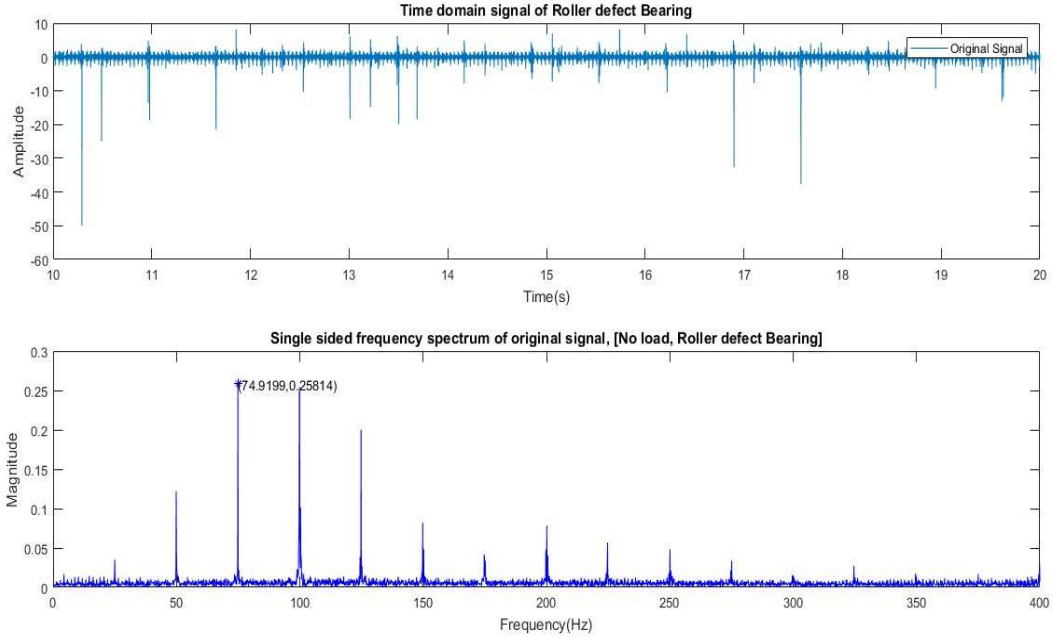

Figure 18. Time domain and FFT graph plot of single roller defect bearing

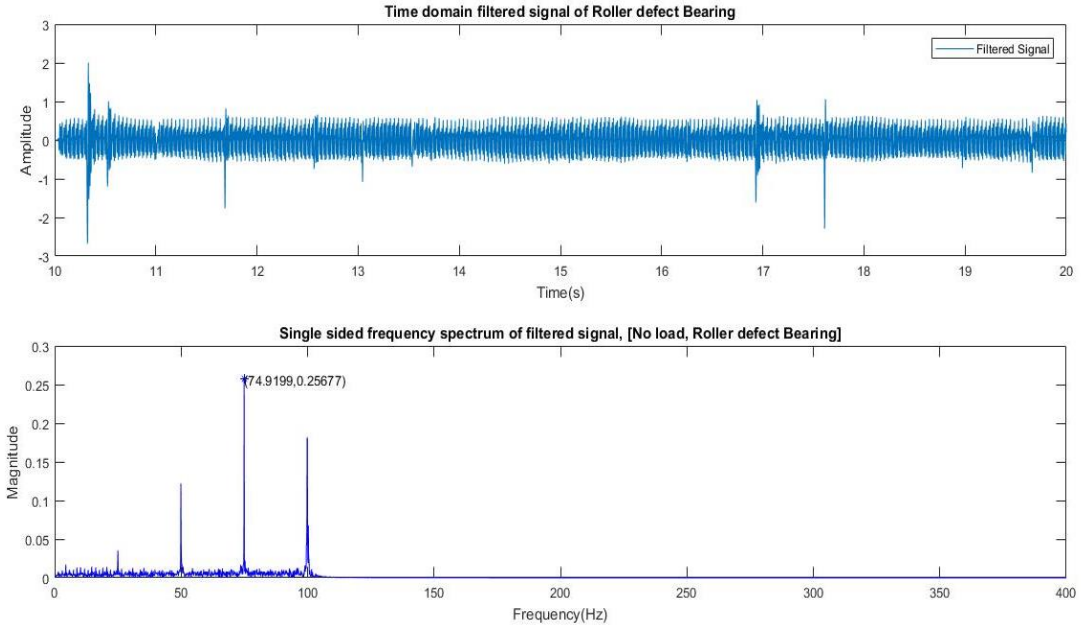

Figure 19. Butterworth filter of single roller defect bearing

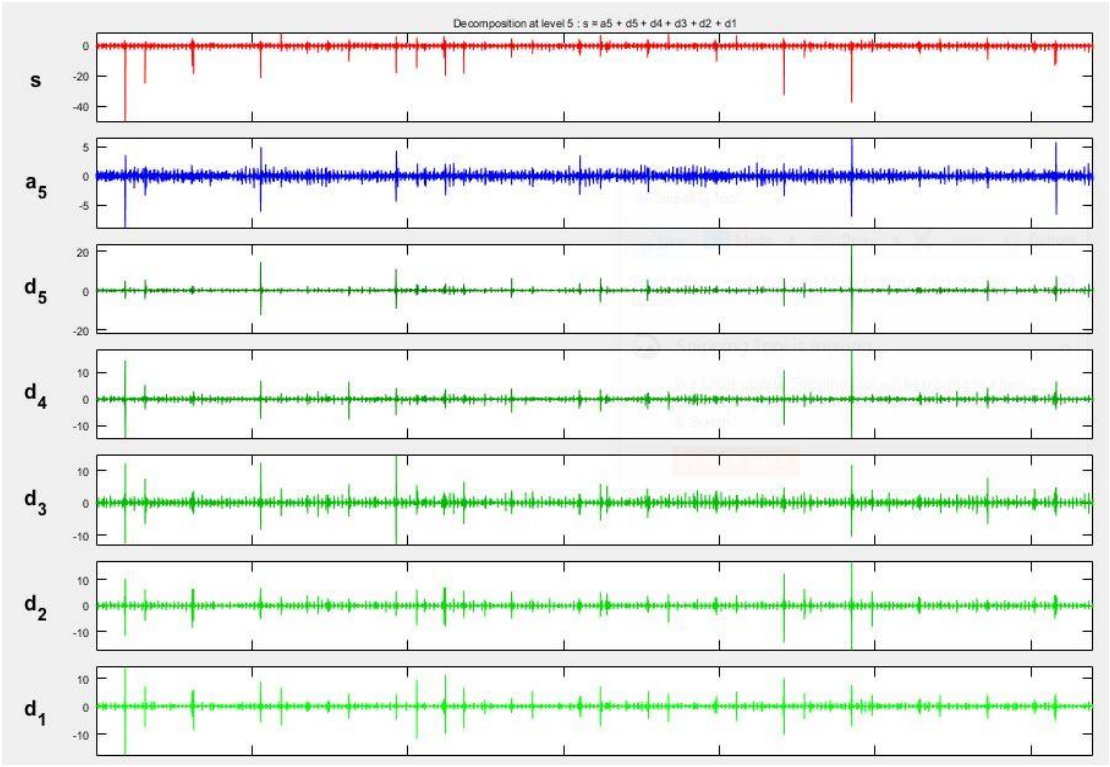

Figure 20. Wavelet decomposition of single roller defect bearing

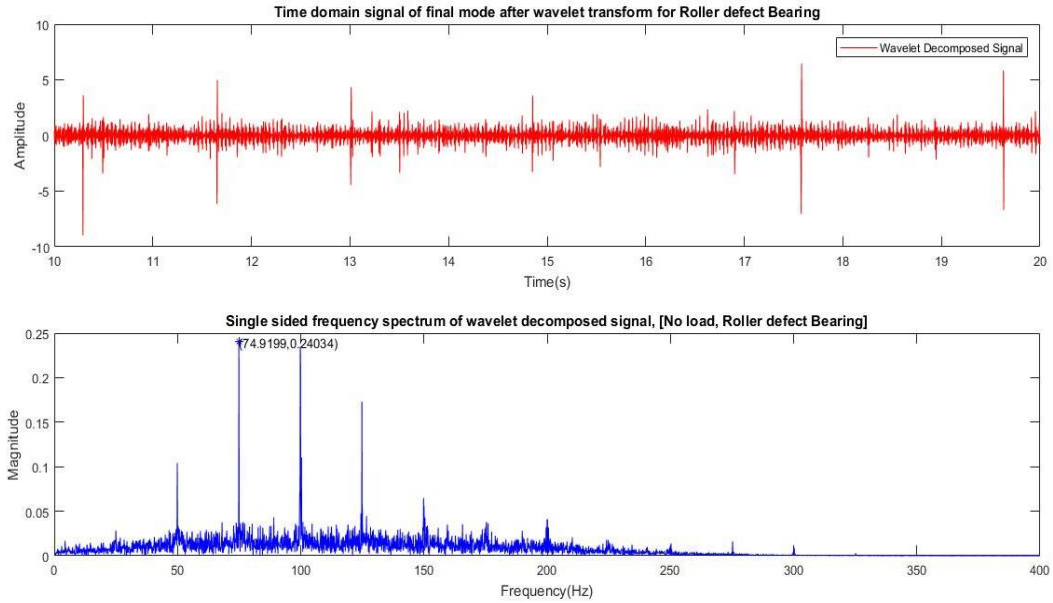

Figure 21. Wavelet decomposed time domain and FFT graph plot of processed signal of single roller defect bearing

6.1.4 Fault condition 2- Outer race defect

The fault is induced on the outer race of a healthy bearing through EDM cut of depth 1mm. The data of faulty bearing can be observed. The time domain vibration signal and its frequency spectrum are shown in fig. 17. The butterworth filter as highlighted in fig. 18 and the wavelet decomposed stages as highlighted in fig. 19 are examined for efficiency. The de-noised signal as well as its frequency spectrum are shown in fig. 20. The peak amplitude after 5 modes of decomposition is observed at frequency of 171.7089 Hz as show in fig. 20 this frequency corresponds with BPOF of the bearing and therefore indicates presence of defect on outer race. The final signal clearly represents outer ring fault of experimental bearing. The comparison of butterworth filter and the wavelet decomposed modes depicts that the wavelet transform stores more harmonics of frequency, hence superior.

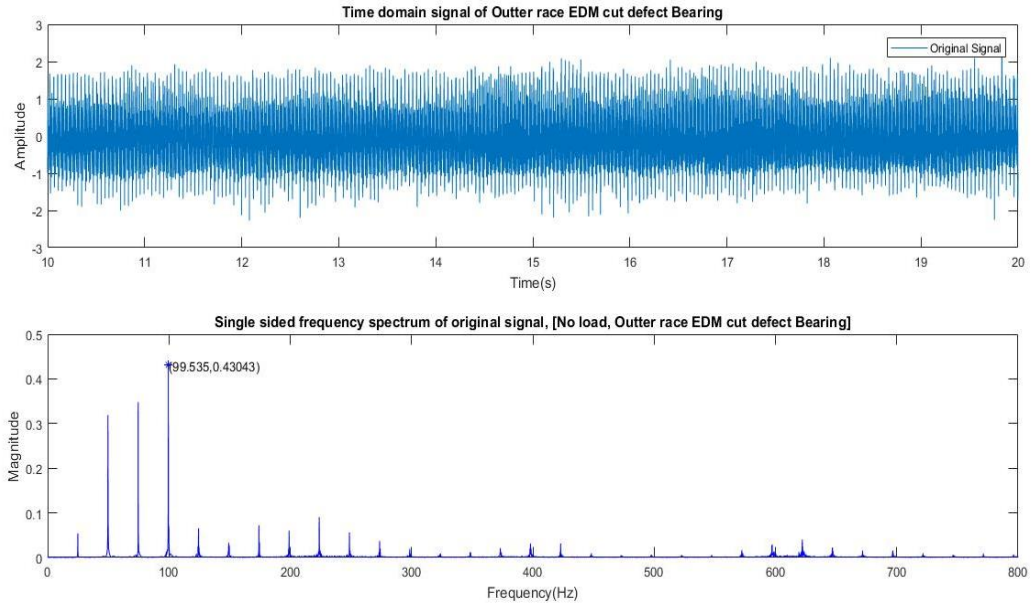

Figure 22. Time domain and FFT graph plot of outer race defect bearing

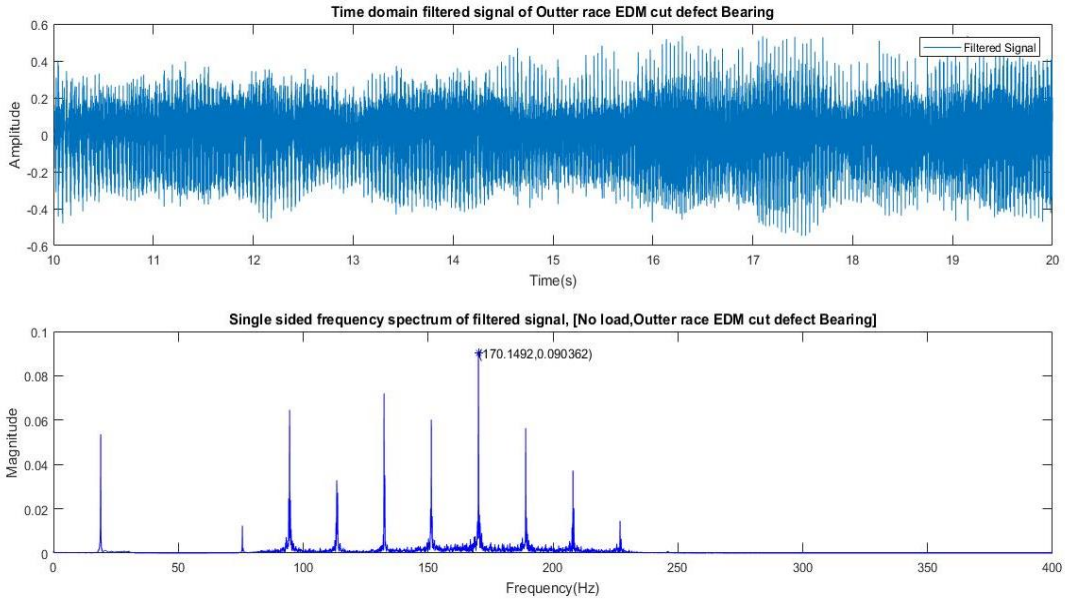

Figure 23. Butterworth filter of outer race defect bearing

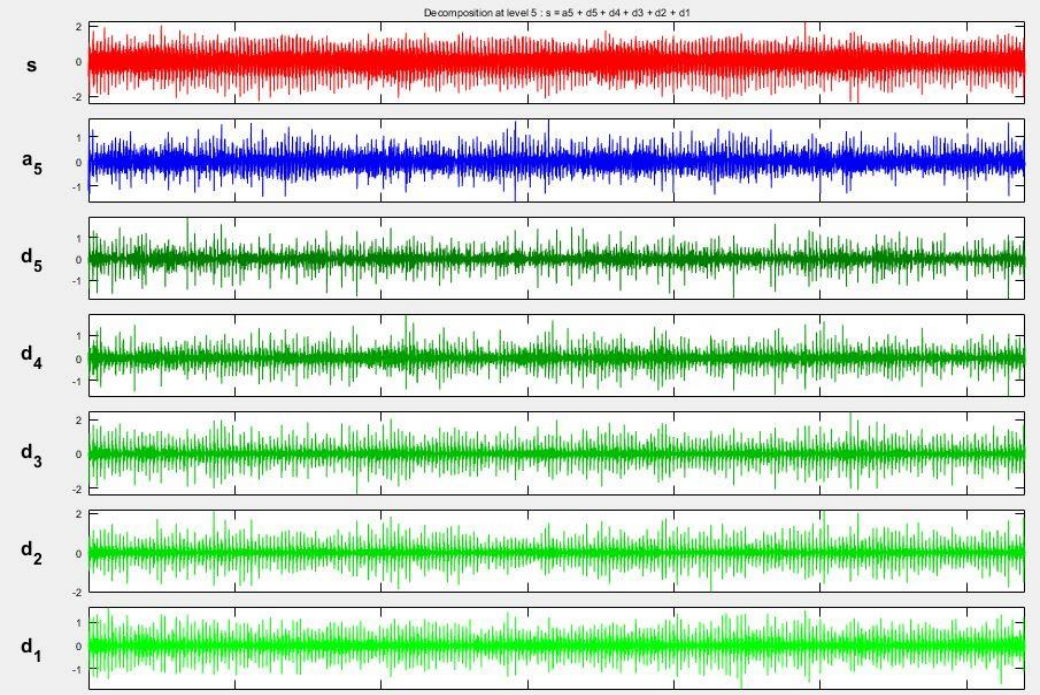

Figure 24. Wavelet decomposition of outer race defect bearing

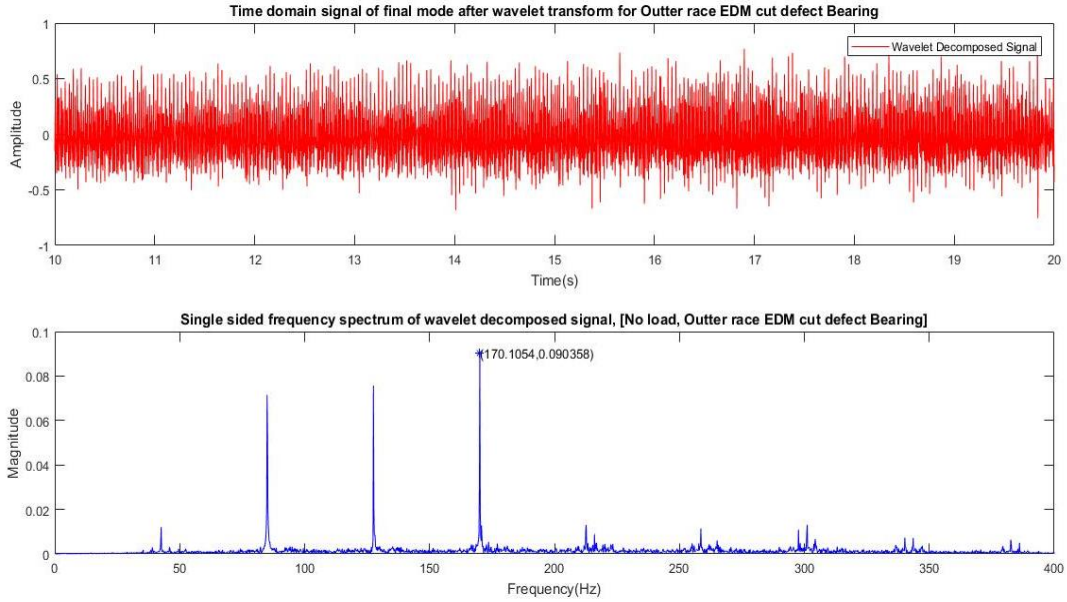

Figure 25. Wavelet decomposed time domain and FFT graph plot of processed signal of outer race defect bearing

6.1.5 Fault bearing condition 3- Double roller defect

The fault is induced on two roller using grinding wheel. The data of faulty bearing can be observed. The time domain raw signal and its FFT spectrum are displayed in fig.21. The butterworth filter as shown in fig. 22 and the wavelet decomposed modes are highlighted in fig. 23 are examined for efficiency. The peak amplitude after 5 modes of decomposition is observed at frequency of 74.4315 Hz as show in fig. 24 this frequency corresponds with BFS of the bearing and therefore indicates presence of defective rollers. The final signal clearly represents roller fault of experimental bearing. The comparison of butterworth filter and the wavelet decomposed modes shows that the wavelet transform stores more harmonics of frequency, hence superior.

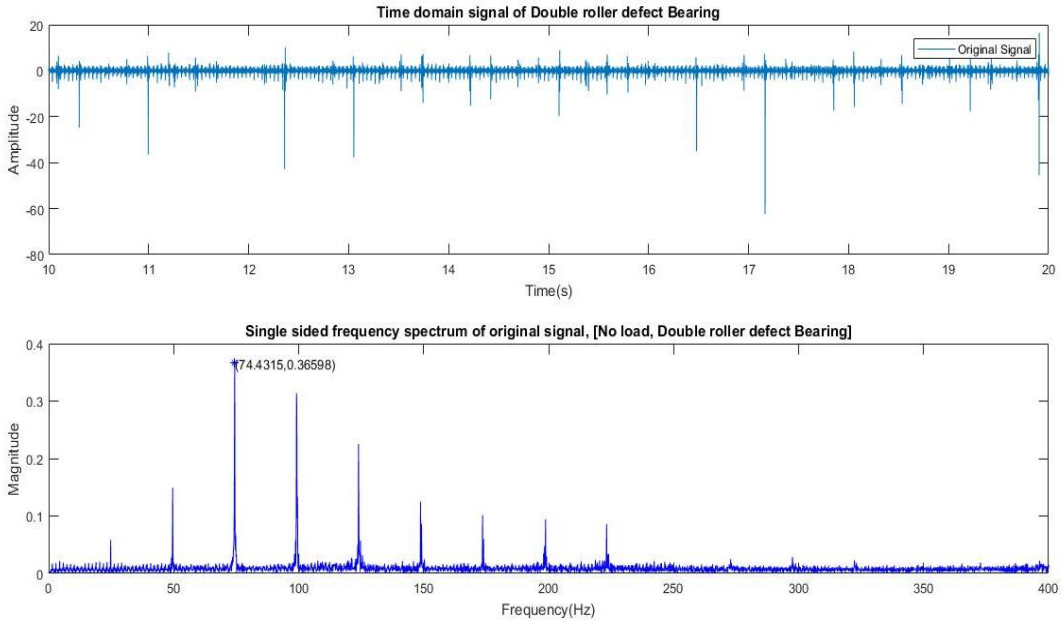

Figure 26. Time domain and FFT graph plot of double roller defect bearing

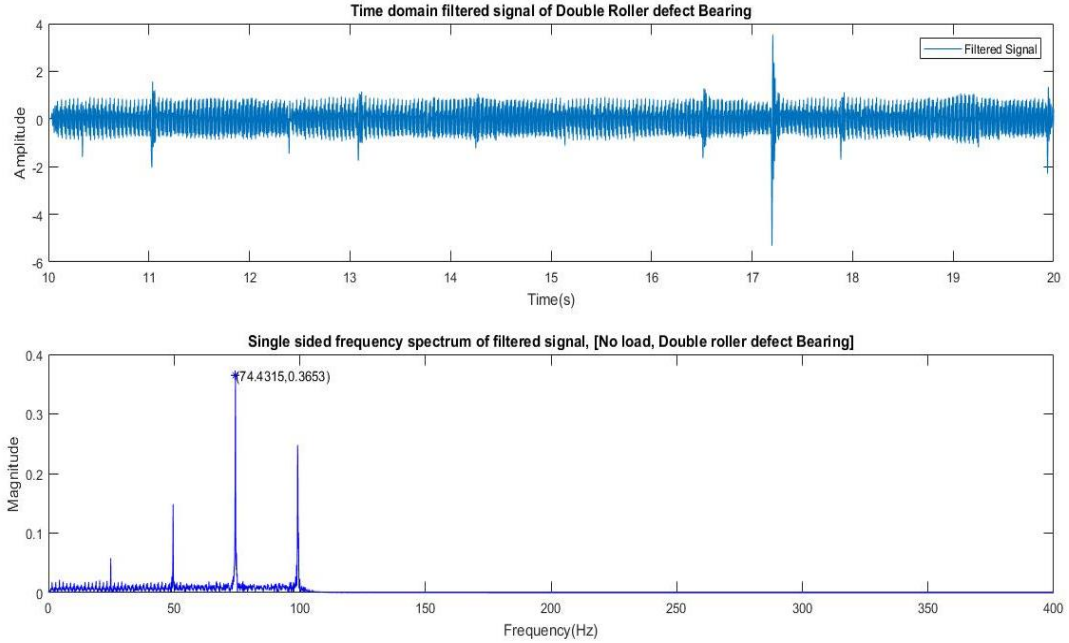

Figure 27. Butterworth filter of double roller defect bearing

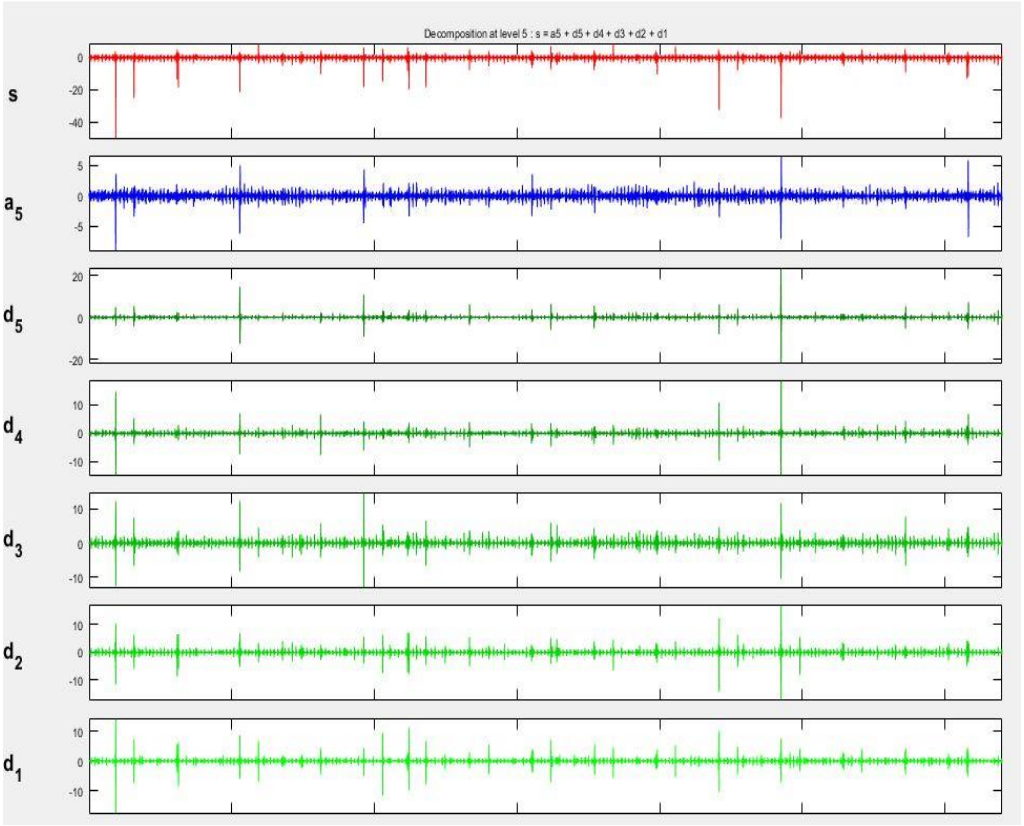

Figure 28. Wavelet decomposition of double roller defect bearing

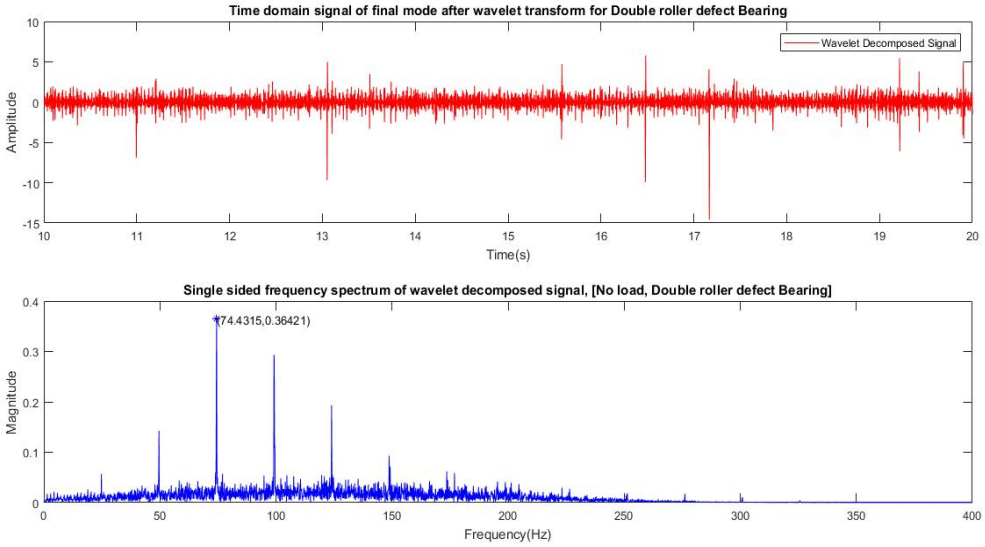

Figure 29. Wavelet decomposed time domain and FFT graph plot of processed signal of double roller defect bearing

6.1.6 Fault bearing condition 4- Inner race defect

The fault is induced on inner race through EDM cut of 1mm depth. The data of faulty bearing can be observed. The time domain raw signal and its FFT plot are shown in fig.25. The butterworth filter as highlighted in fig. 26 and the wavelet decomposed modes are highlighted in fig. 27 are examined for efficiency. The peak amplitude after 4 modes of decomposition is observed at frequency of 232.1442 Hz as highlighted in fig. 28 this frequency corresponds with BPIF of the bearing and therefore indicates presence of defect on the rollers. The final signal clearly represents inner race fault of experimental bearing. The comparison of butterworth filter and the wavelet decomposed modes shows that the wavelet transform stores more harmonics of frequency, hence superior.

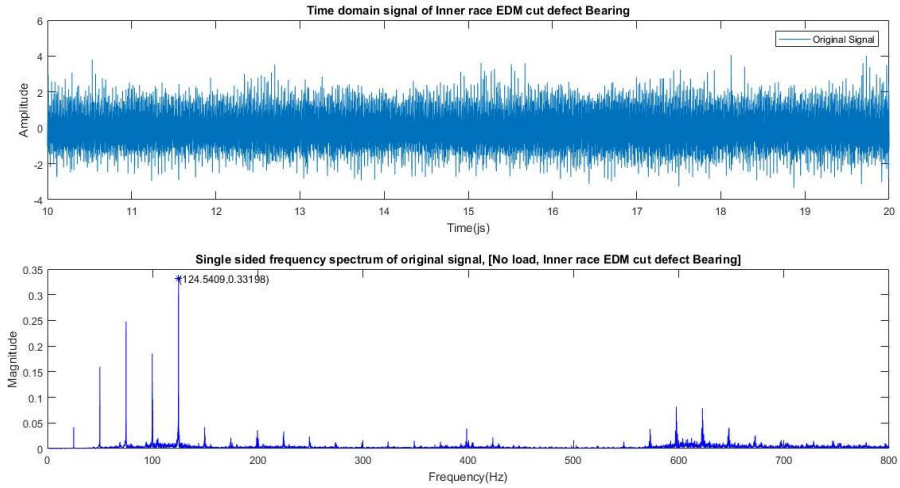

Figure 30. Time domain and FFT graph plot of inner race defect bearing

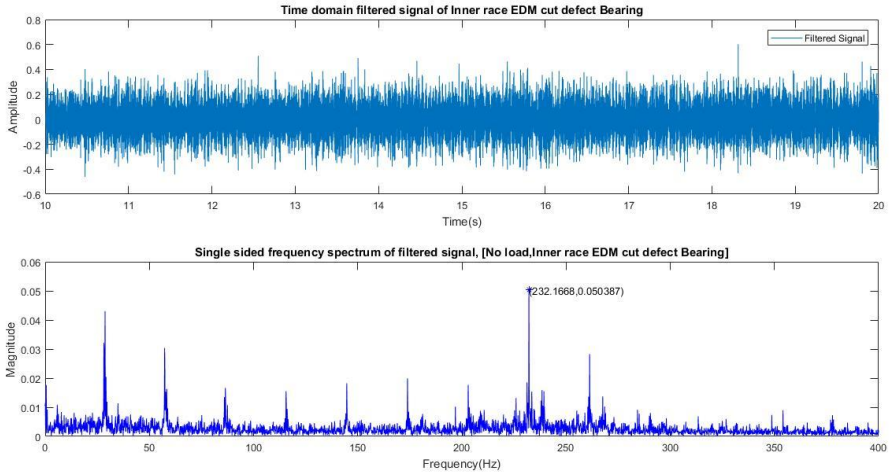

Figure 31. Butterworth filter of inner race defect bearing

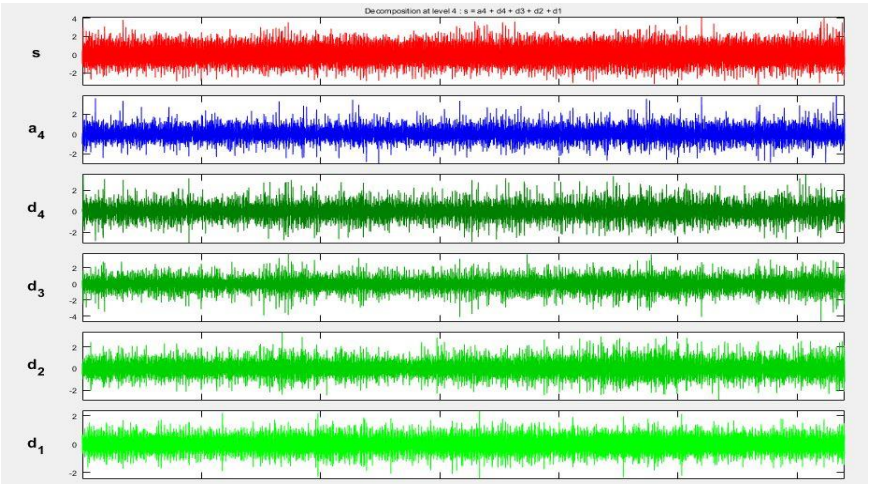

Figure 32. Wavelet decomposition of inner race defect bearing

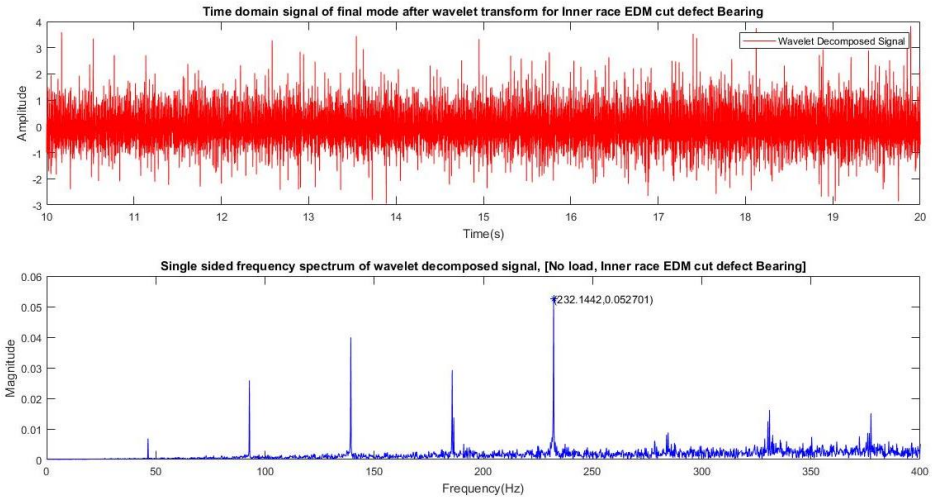

Figure 33. Wavelet decomposed time domain and FFT graph plot of processed signal inner race defect bearing

Table 2. Summary of results obtained from Biorthogonal wavelet transform

Bearing Condition	Amplitude [m/s^2]	Frequency [Hz]
Healthy Bearing	0.04321	24.908
Fault 1	0.24034	74.9199
Fault 2	0.09036	170.1054
Fault 3	0.36421	74.4315
Fault 4	0.05270	232.1442

6.1.7 Bearing with Load conditions [no load, 100gms, 200gms, 300gms]

Table 3. Summary of healthy bearing load

Condition of load	Amplitude [m/s^2]	Frequency [Hz]
No load	0.04321	24.908
100gms	0.04275	24.91
200gms	0.04504	24.91
300gms	0.04171	24.91

The signal processing of healthy bearing concluded peak at natural frequency at 24.9 Hz approximately. All the values in table 3 are highlighted after de-noising the original signal using wavelet decomposition.

Table 4. Summary of single roller bearing defect load

Condition of load	Amplitude [m/s^2]	Frequency [Hz]
No load	0.24034	74.9199
100gms	0.3028	74.63
200gms	0.2857	74.53
300gms	0.29278	74.439

The signal processing of single roller defect bearing concluded peak at BFS at 74.9 Hz approximately. All the values in table 4 are highlighted after de-noising the original signal using wavelet decomposition. As observed from the table 4., a steady decrement in frequency value corresponding to load conditions is indicating the load change.

Table 5. Summary of double bearing defect load

Condition of load	Amplitude [m/s^2]	Frequency [Hz]
No load	0.36421	74.4315
100gms	0.4239	74.3713
200gms	0.3999	74.3299
300gms	0.4098	74.2091

The signal processing of double roller defect bearing concluded peak at BFS at 74.4 Hz approximately. All the values in table 5 are highlighted after de-noising the original signal using wavelet decomposition. As observed from the table 5., a steady decrement in frequency value corresponding to load conditions is indicating the load change.

Table 6. Summary of outer race bearing defect load

Condition of load	Amplitude [m/s^2]	Frequency [Hz]
No load	0.09036	170.1054
100gms	0.1102	169.5936
200gms	0.12892	169.2930
300gms	0.09957	168.7916

The signal processing of outer race bearing defect concluded peak at BPOF at 170.1 Hz approximately. All the values in table 6. are highlighted after de-noising the original signal using wavelet decomposition. As observed from the table 6., a steady decrement in frequency value corresponding to load conditions is indicating the load change.

Table 7. Summary of inner race bearing defect load

Condition of load	Amplitude [m/s^2]	Frequency [Hz]
No load	0.05038	232.1442
100gms	0.0602	231.5936
200gms	0.05892	231.2930
300gms	0.05957	230.7916

The signal processing of inner race bearing defect concluded peak at BPIF at 232 approximately. All the values in table 7. are highlighted after de-noising the original signal using wavelet decomposition. As observed from the table 7., a steady decrement in frequency value corresponding to load conditions is indicating the load change.

6.1.8 Acoustic Emission Signal of healty bearing

Using the ICP 130E20 microphone, the acoustic time domain signal are captured. The procedure for attaining processed singal is same as vibration signal. The time domain signal for healthy bearing is de-noised using band pass filter designed using Matlab's

signal processing toolbox. The cut-off frequency are set according to FFT graph of original signal. From the figure. The signal are de-noised and the peak can be observed at 24.91 Hz which is comparable to natural frequency of taper roller bearing.

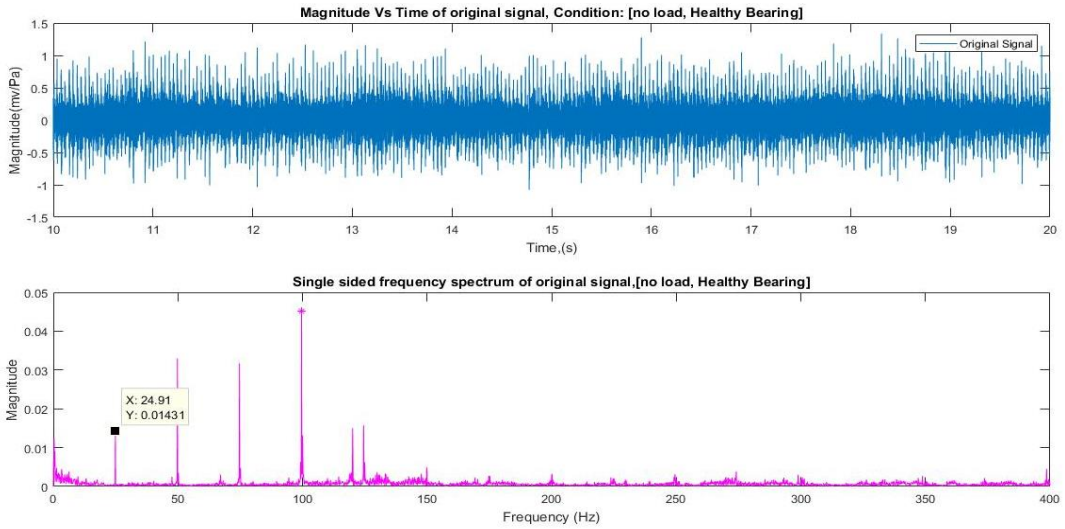

Fig .34 Time domain signal and frequency domain graph of healthy bearing acoustic emission

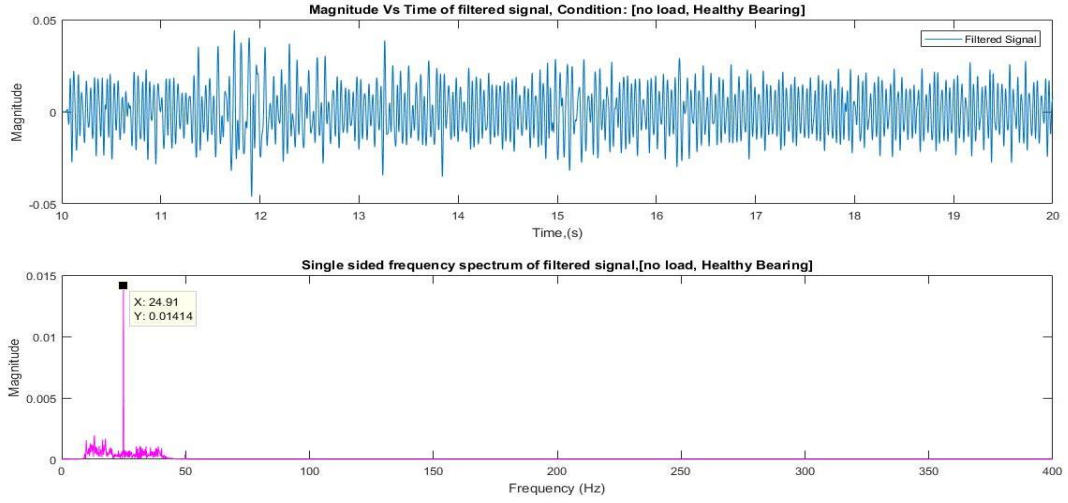

Fig. 35 Filtered time domain and frequency domain signal of healthy bearing

6.1.9 Acoustic Emission Signal of single roller bearing

The acoustic time domain signals of single roller bearing defect are captured. The procedure for attaining processed singal is same as vibration signal. The time domain

signal for roller defect bearing is de-noised using band pass filter created using Matlab's signal processing toolbox. The cut-off frequency are set according to FFT graph of original signal.

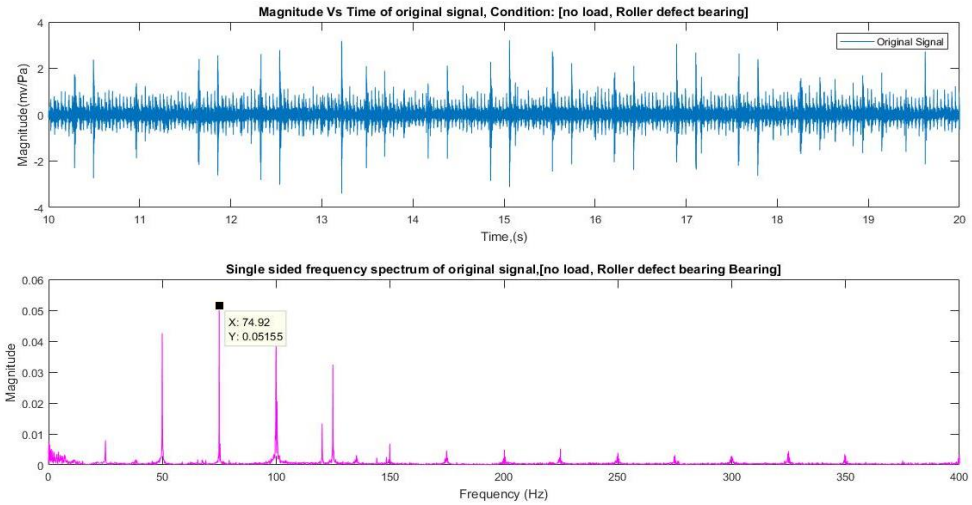

Figure. 36 Time domain signal and frequency domain graph of roller bearing defect acoustic emission

From the figure. The signals are de-noised and the peak can be observed at 74.92 Hz which is comparable to BFS characteristic frequency of taper roller bearing.

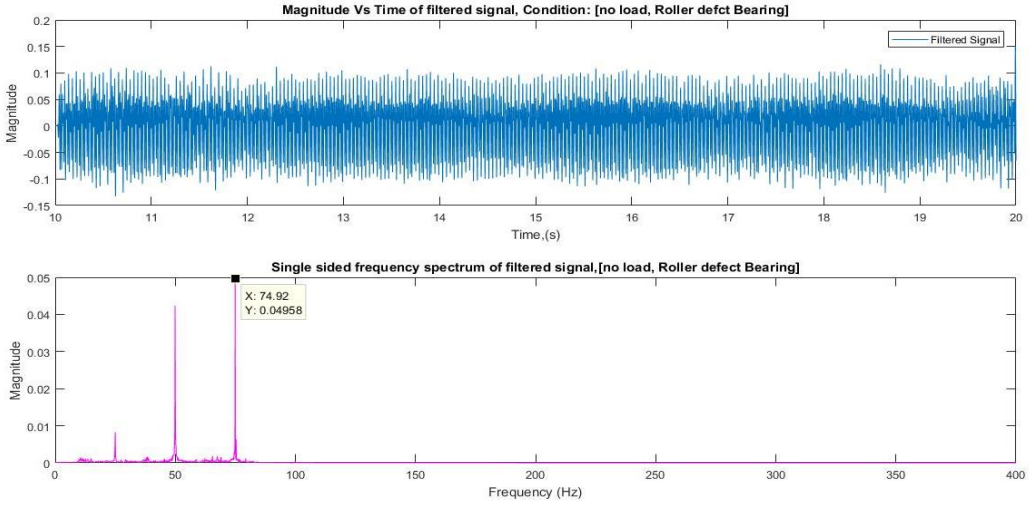

Figure. 37 filtered time domain and frequency domain signal of roller bearing defect

CHAPTER 7

RESULTS AND DISCUSSION

7.1 Vibration fault classification

(a) Automatic classification of fault using Artificial Neural Networks (ANN)

ANN is employed to facilitate automatically classify faults for various bearing fault conditions. This is done through MATLAB's deep learning toolbox which includes a pattern recognition neural network specifically designed to help recognise and classify patterns in data that is supplied to the network. Pattern recognition neural networks used for this purpose are basically feed forward networks consisting of a hidden layer containing a pre-set number of hidden neurons and a SoftMax layer that are trained to classify input data matrix according to target matrix. The target data matrix is a column matrix which should have a 1 value corresponding to the class it belongs to. The hidden neurons given are equal to 8 as it is ideally between 10 and 5 which corresponds to input layers and output layers respectively.

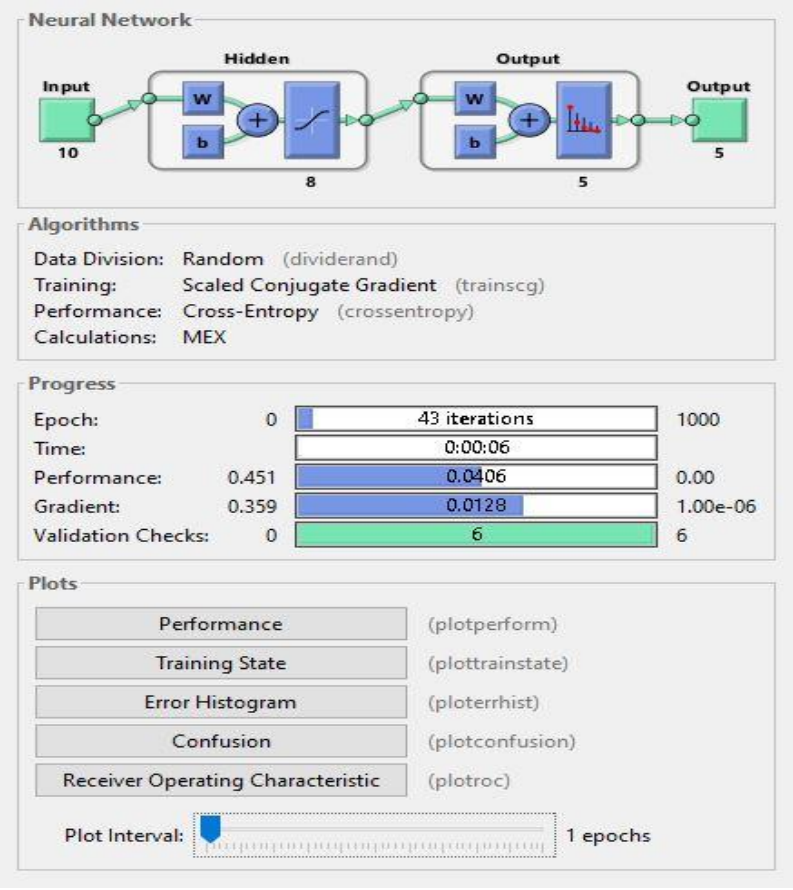

Figure 38. ANN data

The training function or algorithm used for the network is a resilient backpropagation learning function that changes weights and biases by the rules of the resilient backpropagation algorithm. The resilient backpropagation algorithm is known to be faster than normal back propagation and also is more efficient for pattern recognition applications. The maximum epochs, minimum gradient and maximum validation checks are set to default setting which are 1000, 1e-5 and 6 respectively. The input data matrix consisting of 10 extracted features, 5 different bearing conditions including healthy condition are supplied as inputs. The confusion plot, performance plot, training state graph and error histogram are obtained to analyse the success of the neural network implementation.

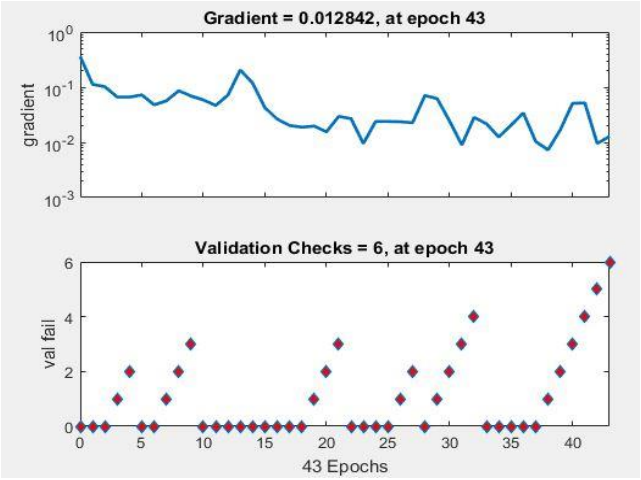

Figure 39. Training state performance

The training state graph in Fig. 30 shows the current progress/status of the training at a specific time while training is in progress. Since the default setting of 6 validation checks is used the training stops when 6 validation checks are completed.

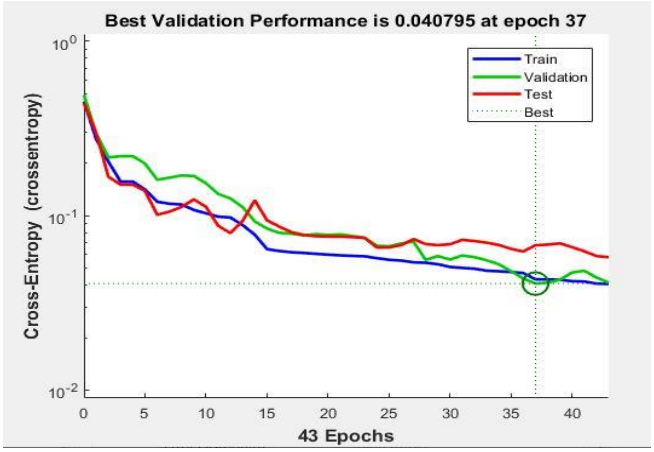

Figure 40. Performance diagram

The performance plot shown in Fig 31 shows mean squared errors vs epoch for training, validation and test performance of the training process. The errors are shown to decrease after more epochs of the training. As per setting of 6 validations check the training ends 6 increases in validation error and the best performance is indicated at the epoch with lowest validation error

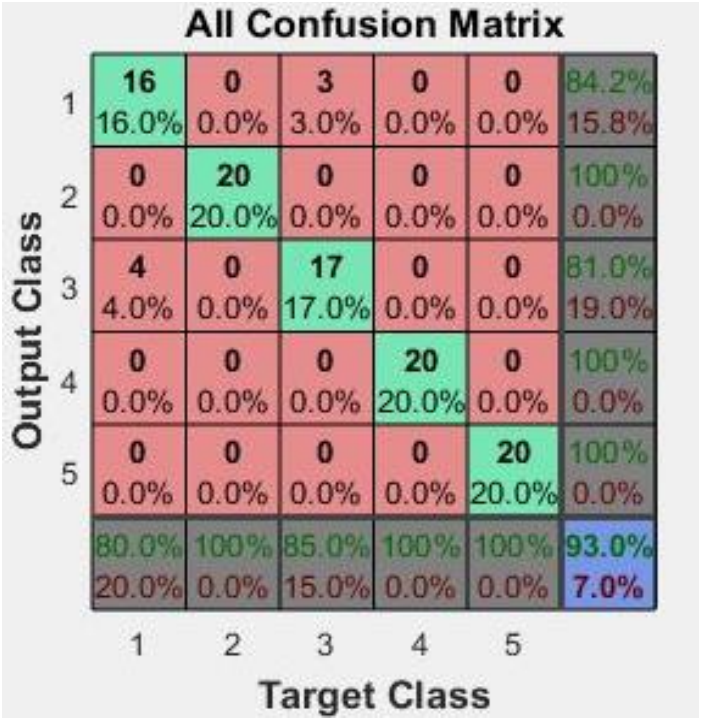

Figure 41. Confusion Matrix

From confusion matrix shown in Fig 32 the success rate of the network is obtained as 93% at the end of 48 iterations. The diagonal matrix represents the classification of faults

with true class match. the error occurs the most by the classifier are shown as the off-diagonal cell. The percentage of accuracy by each fault classification are highlighted at the top right corner plus the bottom left corner shows the percentage achieved by predicted class.

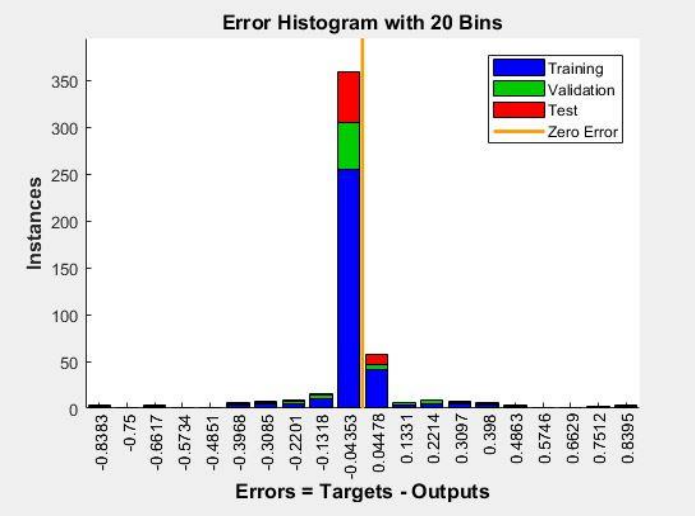

Figure 42. Error histogram

Error histogram shown in Fig.33 represents errors that approach to Mean Squared Error (MSE). This is plotted by dividing the total error range of the neural network into 20 bins. Each bin corresponds to a bar in the graph which has a width of total error range divided by 20. It shows that less than 250 instances were used for training purpose and approximate 50 each for validation and testing process obtaining a success of 0.04353 error only.

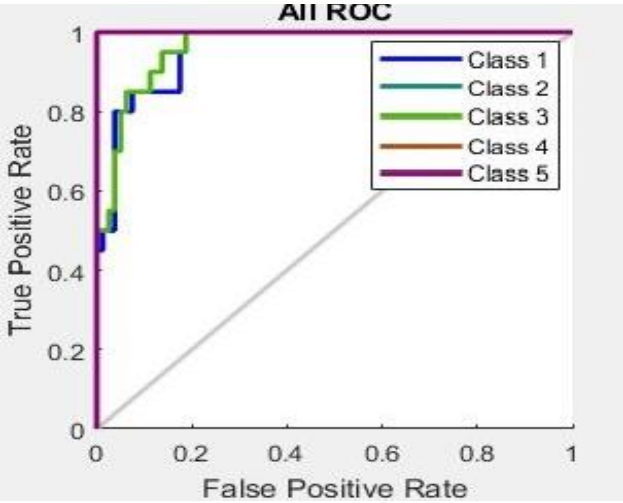

Figure 43. ROC plot

The ROC plot plots the receiver operating characteristic for every one of the bearing condition or categories. The better closeness of each line to the top left corner of the plot the more successful the differentiation between classes.

(b) Automatic classification of fault using Deep Neural Networks (DNN)

In order to achieve better accuracy in classification DNN is applied the data set matrix of extracted features and their classes. Through research it is known that DNN with multiple hidden layers show better result for classification of data which is complex. At multiple layers, different features help in abstraction to denoise the signal.

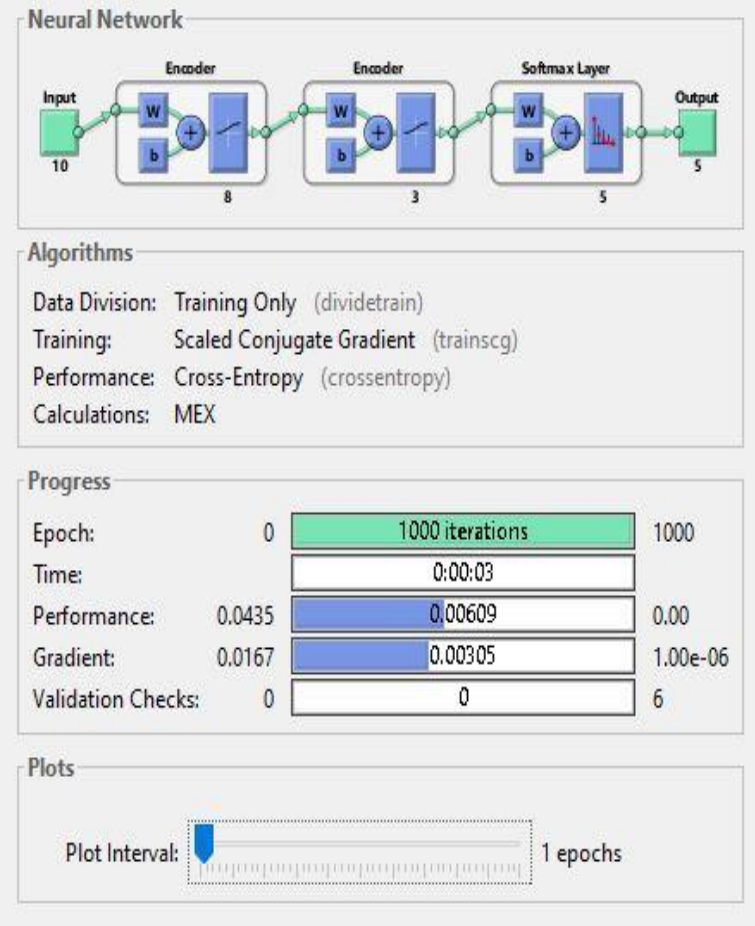

Figure 44. DNN

The deep neural network was constructed using two autoencoder layers and one softmax layer. Autoencoders were chosen to make it convenient to train one layer at a time which would otherwise be difficult. The process involves train two hidden layers

separately using re set training functions, epochs and other properties using autoencoders. After this a final softmax layer is trained. These separate layers are stacked together to form a single deep neural network which is train one for the last instance to obtain the results. As the varying nature of the input data set various properties/settings of the train autoencoder function in MATLAB's deep learning toolbox. These included impact of the regularizer for the weights of the network to 0.001 as this should typically be small, the sparsity regularizer was set to 0.05 this helps enacting a condition on the sparsity of the output from the hidden layer, sparsity proportion which controls the sparsity of the result as compared to the hidden layer is set to 0.05. An appropriate linear transfer function was used for the decoder of each hidden layer. The middle layer size of 1st layer is chosen as 8 as it is required to be less than the input layer size to avoid overfitting of the network. The middle layer size of the second layer is set to 3 which should be close to half of the first layer so that the second encoder learns a less big presentation of the input data. The features generated from the 1st are used to train the 2nd hidden layer.

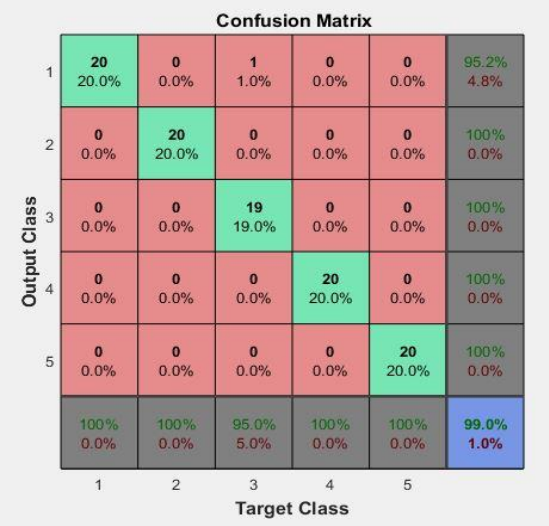

Figure 45. Confusion matrix

The confusion matrix highlighted in Fig.36 depicts that an accuracy of 99% is obtained which is more comparable to the success rate in ANN. The performance plot shown in Fig 37 shows mean squared errors vs epoch for training, test and validation check performance of the training process. The best training performance reaches at 1000 epochs.

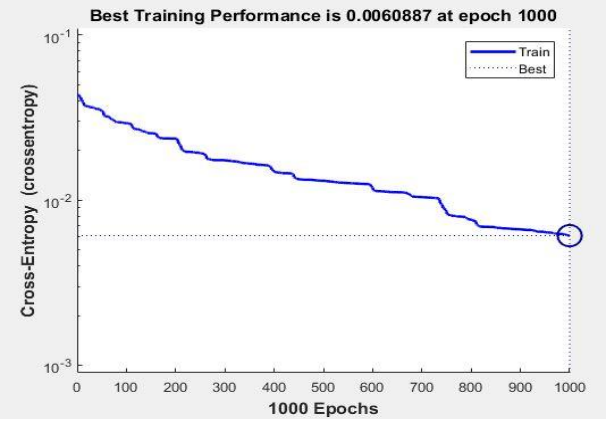

Figure 46. Performance plot

As seen from the graphs the number of network iterations to train the network are significantly high due to complex architecture and a greater number of neurons. Other plots i.e. performance, training state, error histogram and ROC are shown to compare the various properties depicting the performance of the network.

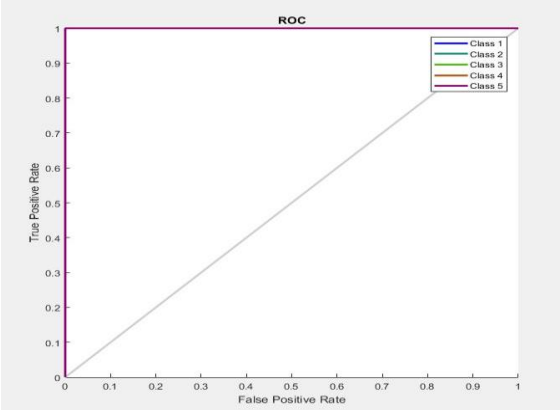

Figure 47. ROC

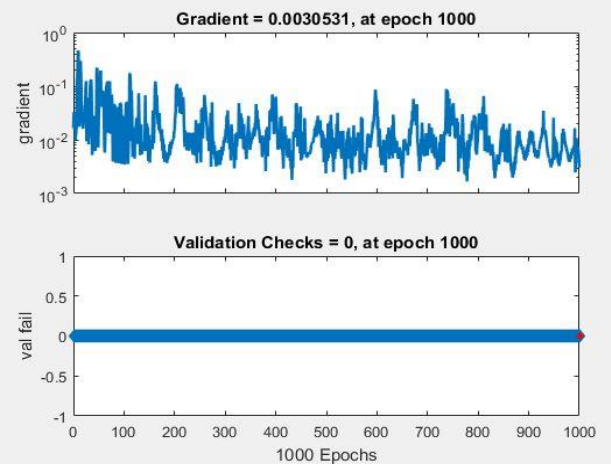

Figure 48. Training plot

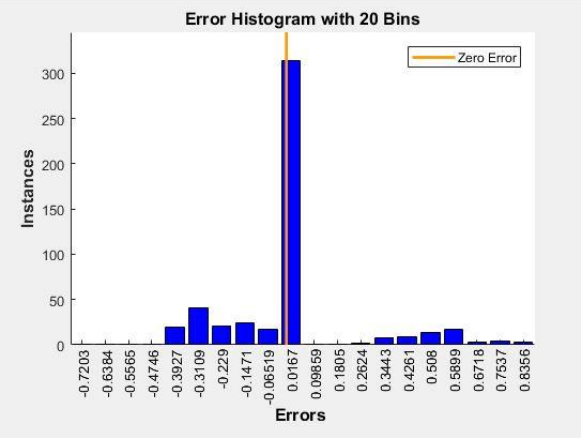

Figure 49. Error histogram

7.2 Acoustic emission fault classification

(a) Automatic classification of faults using ANN

The ANN for classification of 5 bearing cases were designed in a similar way as done in the case of vibration data. The input matrix was formed containing information about the 10 extracted features for 100 samples each corresponding to 10 seconds of data. 20 samples were taken for every one of the 5 bearing cases. The target matrix was formed in a similar way to assign value 1 to the class the sample belongs to. The default ANN patternet settings were used for the classifier and it took 40 iterations to train the network to obtain the highest accuracy of 96%.

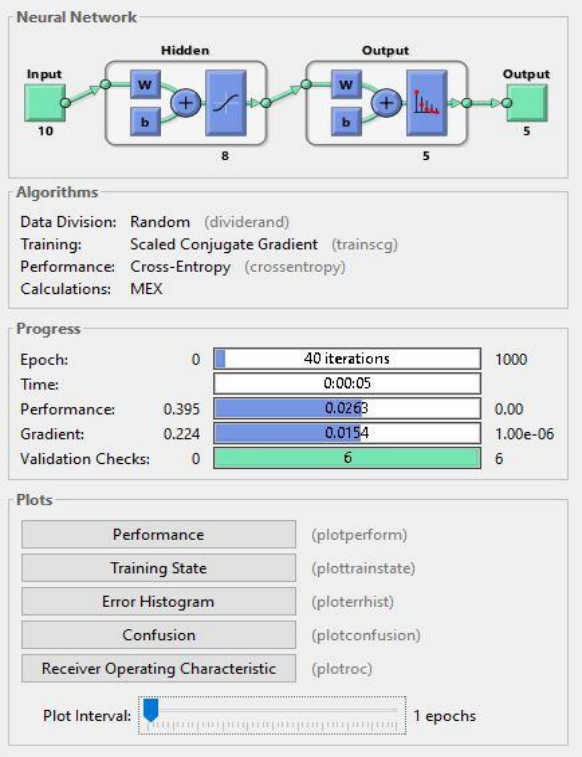

Figure 50. ANN

The confusion plot in fig. 46 represents the classification between different cases the bottom right corner shows the overall accuracy. The diagonal elements display the percentage of samples that were classified correctly whereas the non-diagonal cells represent the elements which were not classified correctly. It can be seen that most of the misclassifications were between classes 1, 3 and 4 which represented the healthy, outer ring effect and inner ring defect respectively. This indicates that the feature value for these cases are somewhat similar and thus the neural network fails to identify a pattern while the roller defect feature values are easily distinguishable.

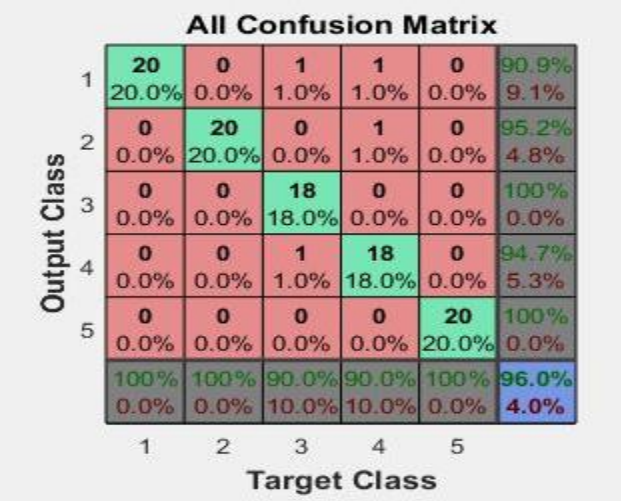

Figure 51. Confusion matrix

The training state graph in Fig. 47 shows the current progress/status of the training at a specific time while training is in progress. Since the default setting of 6 validation checks is used the training stops when 6 validation checks are completed. This can be compared with the training state plot of the ANN of vibration data in Fig. 30.

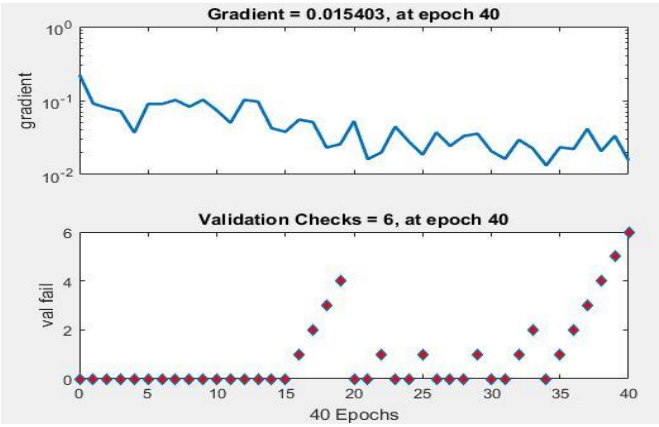

Figure 52. Testing plot

The performance plot shows the cross entroy vs epochs(iterations). The cross entropy represent he mean squared errors. It can be seen how the different lines decrease with the incrase in number of iterations i.e. blue representing the training error, green validation and red test error.. The training stops after 6 validation errors as per default settings of network which is taken as the best possible state and plot ends where atleast one of the line coincides with the best condition as per settings of the network.

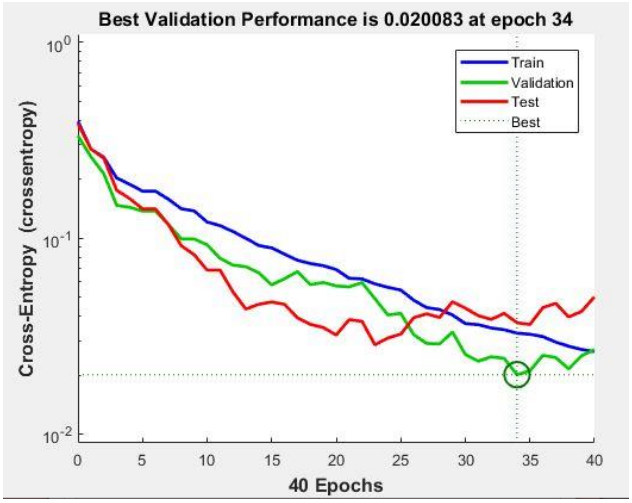

Figure 53. Performance plot

The error histogram(Fig. 49) further highlights the success of the netwok error as most error instaces lie near the zero error line where arounf 275 instances are used for trainging alone which is more than the part used in testing and validation.

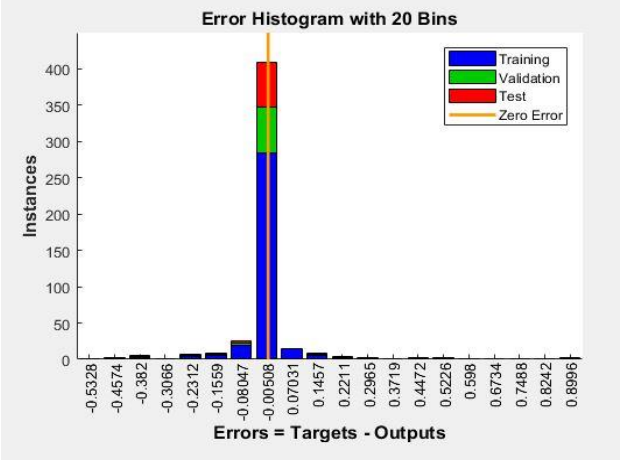

Figure 54.. Error Histogram

The ROC plot plots the receiver operating characteristic for every one of the bearing condition or categories. The better closeness of each line to the top left corner of the plot the more successful the differentiation between classes. Here the ROC plots for all 3 steps

i.e. testing training, training and validation can be seen. The performance of testing and validation is good as the area enclosed by lines in top left corner is close to zero.

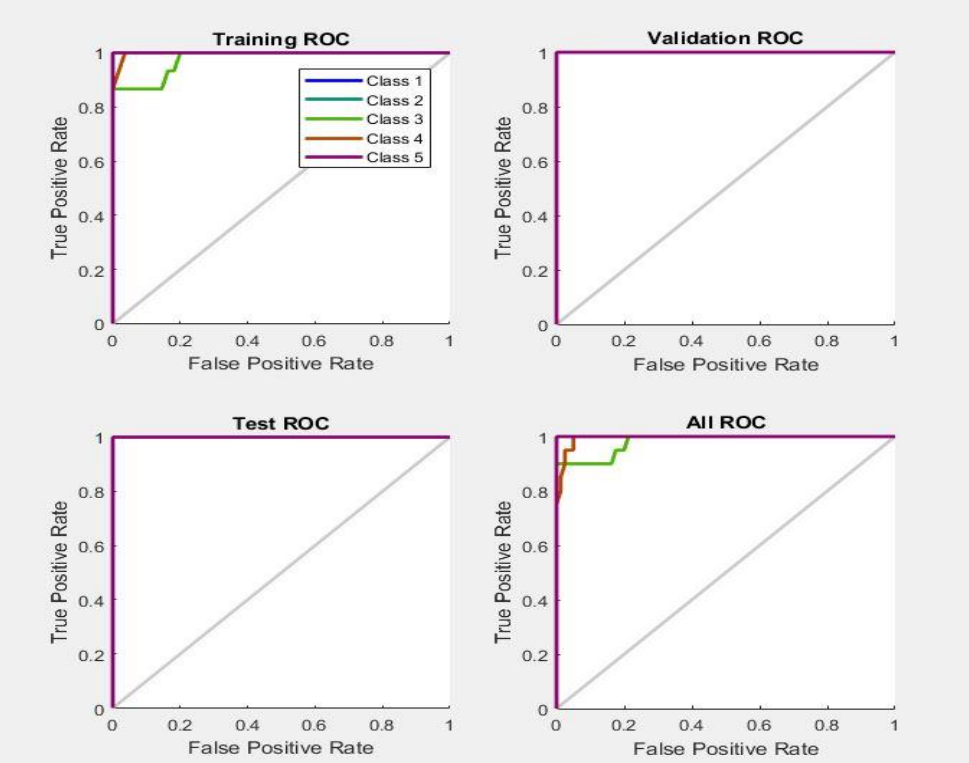

Figure 55. ROC plot

(b) Automatic classification of fault using DNN

In case of DNN design it was found that the best training performance occurs when the number of hidden neurons in first and second auto encoder layers were taken as 8 and 6 respectively. 100 iterations were taken as maximum so that fair comparison can be made with ANN based training approach. The functioning of the network was same as in the case of DNN with vibration data as all other settings were kept same.

The confusion matrix highlighted in Fig. 51 depicts that an accuracy of 98% is obtained which is more comparable to the success rate in ANN. The performance plot shown in Fig 54 shows mean squared errors vs epoch for training, test and validation check

performance of the training process. The best training performance reaches at 1000 epochs which the maximum allowed iterations as per settings. It was observed the accuracy remains at maximum of 98% even after allowing more iterations.

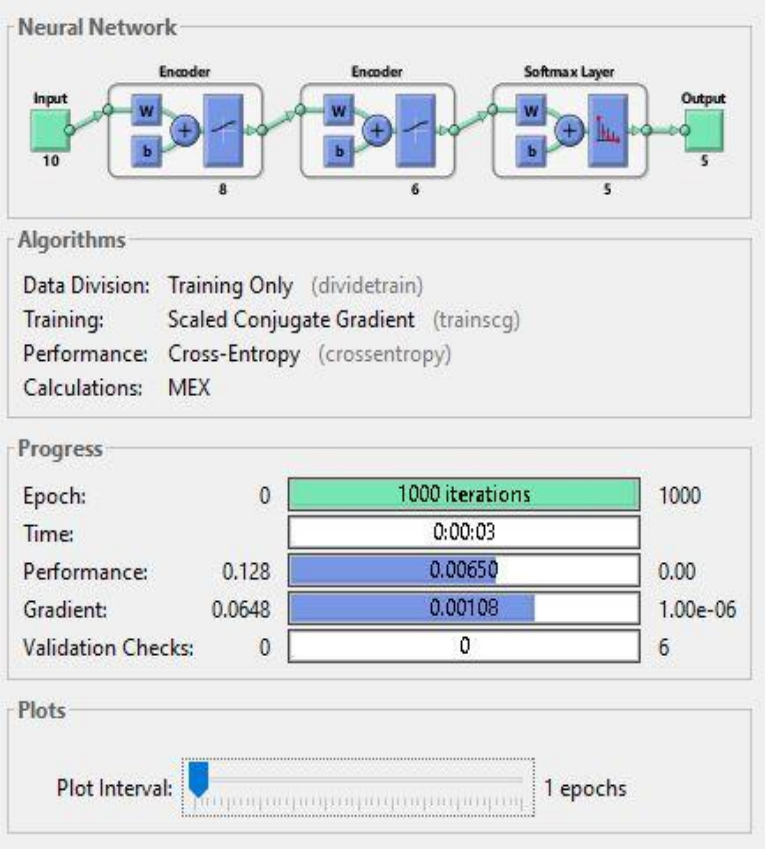

Figure 56. DNN

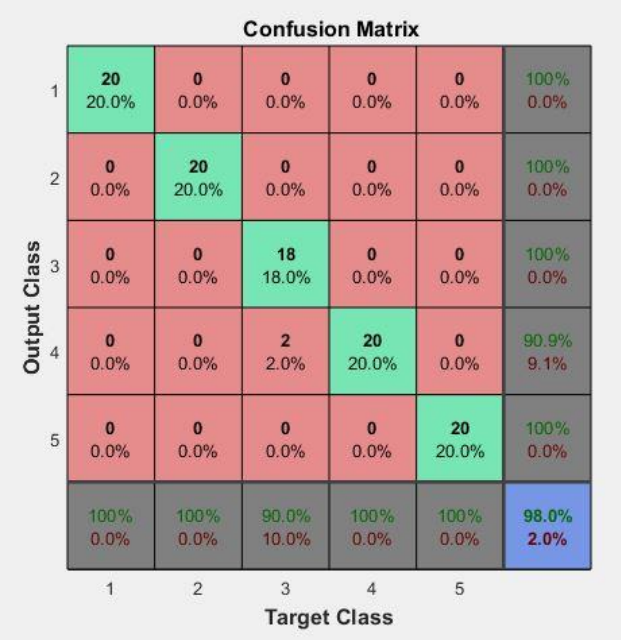

Figure 57. Confusion matrix

As seen from the graphs the number of network iterations to train the network are significantly high due to complex architecture and a greater number of neurons. Other plots i.e. performance, training state, error histogram and ROC are shown to compare the various properties depicting the performance of the network.

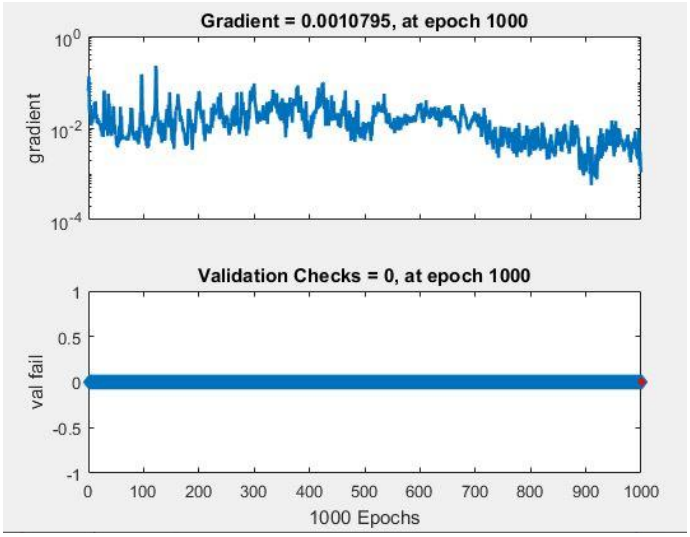

Figure 58. Training plot

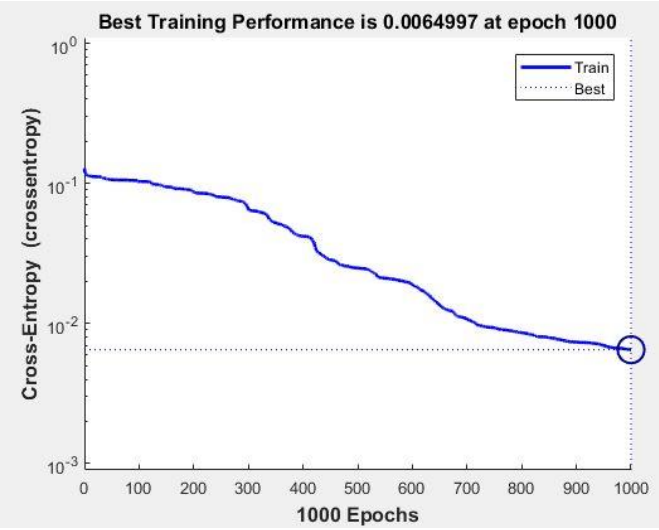

Figure 59. Performance plot

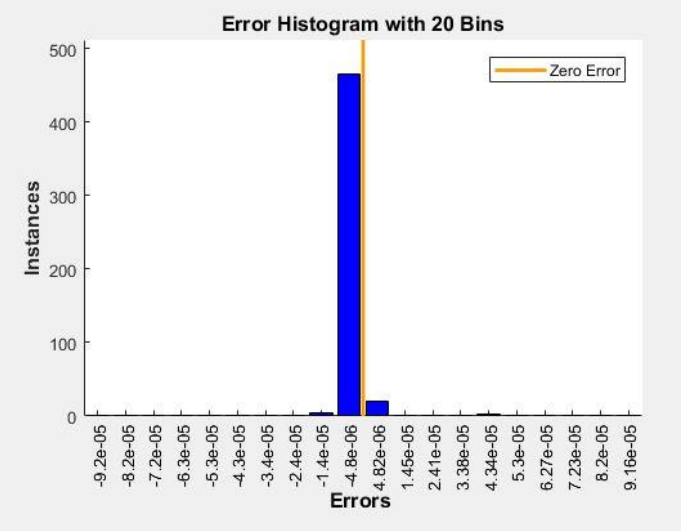

Figure 60. Error histogram

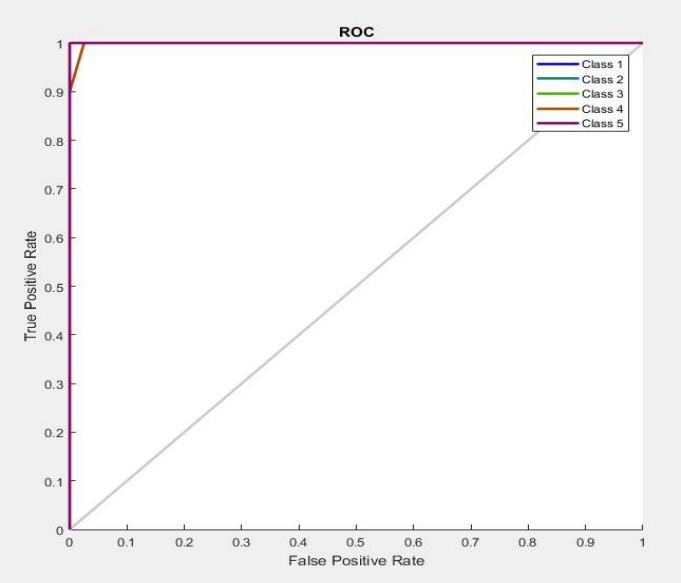

Figure 61. ROC

CHAPTER 8

SUMMARY

8.1 Conclusions

The study is practiced on collecting vibration data and conducting de-noising comparison between low pass Butterworth filter and Biorthogonal wavelet transform. Clearly, due to complexity of multiple mode of wavelet function, biorthogonal wavelet turns out to be precise and accurate in removing the noise as compared to low pass butterworth filter. The wavelet removes the noise by compressing or suppressing the components of detailed coefficients which are made of high frequency noise and characteristic information of the machine fault. Comparing the filter and wavelet, the wavelet de- noising needs area of expertise to create extract the signal as the mode and order have to be varied.

A neural network approach for fault classification is much reliable that previous signal processing techniques as it automatically segregates the outputs whereas the previous pressing techniques required manual fault input to determine the classification. The research shows the advantage of using deep neural network over artificial neural network. The deep neural network easily classifies huge signal output data and accurately identifies the faults. According to the confusion matrix, deep neural network is 99% accurate whereas, artificial neural network achieves 93% accuracy. However, the deep neural network run many more iterations as compared to artificial neural network.

Moreover, along with vibration data acoustic emission data was also collected. It was seen that acoustic emission analysis has equal potential of classifying faults and even better in some cases as the ANN efficiency in the case of acoustic data was observed to be 96% more than that of 93% in the case of vibration data. Therefore, from an industrial application point of view using a system that integrates both vibration and acoustic emission detection functionalities would prove to be beneficial as some faults which may

not be diagnosed by one method may be detected by the other thus full proofing the system. This would also offer greater assurance to the presence of a particular defect type when both the systems independently classify it into the same category.

8.2 Scope for future work

There are many areas which can be explored for future work on the study.

- To prepare a user face interface application where the raw data of a given rotation instrument and formulate the area of fault and classify using the natural characteristic frequency.
- Explore various rotating instrument to detect fault at early stage of damage.
- Automatic detection of fault and circuit integrated halt of the system to reduce any further damage to the assembly.
- Study other signal processing techniques for better and faster results.

CHAPTER 9

REFERENCES

[1] H Saruhan, S Sandemir, A Cicek and I. Uygur (2014), Vibration Analysis of Rolling element bearing defects, *Journal of applied Research and Technology*, Vol. 12, Issue 3, June 2014, pp. 384-395.

[2] Hussein Al-Bugharbee and Irina Trendafilova (2015), A fault diagnosis methodology for rolling element bearings based on advanced signal pretreatment and autoregressive modelling, *Journal of Sound and Vibration,* 369(May 2015), pp. 246-245.

[3] I.M. Jamadar and D.P. Vakharia (2016), A novel approach integrating dimensional analysis and neural networks for the detection of localized faults in roller bearings, *Journal of measurement,* Vol. 94, pp. 177-185.

[4] Jaouher Ben Ali, Nader Fnaiech , Lotfi Saidi , Brigitte Chebel-Morello and Farhat Fnaiech (2015), Application of empirical mode decomposition and artificial neural network for automatic bearing fault diagnosis based on vibration signals, *Journal of applied acoustics,* Vol. 89, pp. 16-27.

[5] Jinglong Chen, Jun Pan, Zipeng Li, Yanyang Zi, Xuefeng Chen (2015), Generator Bearing Fault diagnosis for wind turbine via empirical wavelet transform using measured vibration signals, *Journal of renewable energy*, Vol 89, 80-92.

[6] Narendiranath Babu Thamba, Arun Rakesh, Mohamed Jahzan (2017, Application of EMD, ANN and DNN for self- Aligning bearing fault diagnosis, *Archives of Acoustics*, Vol 43, 2, pp. 163–175 2018.

[7] Narendiranath Babu Thamba, Himanshu H.S., Prabin Kumar N., Rama Prabha D., Nishant C. (2017), Journal Bearing fault detection Based on Daubechies Wavelet, *Archives of Acoustics,* Vol 42, Issue 3, pp. 401-414

[8] OlivierJanssens, ViktorSlavkovikj, BramVervisch, KurtStockman, Mia Loccufier, StevenVerstockt, RikVandeWalle, Sofie VanHoecke (2016), Convolutional Neural

Network Based Fault Detection for Rotating Machinery, *Journal of Sound and Vibration*, Vol. 377, May 2016, pp. 331-345.

[9] O.R. Seryasat, M. Aliyari shoorehdeli, F. Honarvar and Abolfazl Rahmani (2010), Multi-fault diagnosis of ball bearing using FFT, wavelet energy entropy mean and root mean square (RMS), *Proceedings of 2010 IEEE International Conference on Systems, Man and Cybernetic*, pp. 10-13 Oct 2010.

[10] P Shakya, A K Darpe and M S Kulkarni (2013), Vibration-based fault diagnosis in rolling element bearings: ranking of various time, frequency and time-frequency domain data-based damage identification parameters, *Journal of Condition Monitoring*, Vol. 3, Issue 2, Oct 2013.

[11] Pankaj Guptaa and M. K Pradhanb (2016), Fault detection analysis in rolling element bearing, *Proceedings of 5th International Conference of Materials Processing and Characterization (ICMPC 2016)*, pp. 2085-2094.

[12] Rajeswari.C ,Sathiyabhama.B,Devendiran.S & Manivannan.K, (2014), Bearing fault diagnosis using wavelet packet transform, hybrid PSO and support vector machine, *12th Global Congress on manufacturing and management (GCMM 2014)*, Vol. 97, pp. 1772-1783.

[13] Sunnersjö, C. S (1978). Varying compliance vibrations of rolling bearings. *Journal of sound and* vibration, Vol.58, Issue 3, (1978), pp. 363-373.

[14] Wardle FP and Poon SY (1983), Rolling bearing noise — cause and cure, *Journal of Chartered MechEngr*, July/August 1983, pp. 36–40.

[15] V.Hariharan and PSS. Srinivasan (2009), New Approach of Classification of Rolling Element Bearing Fault Artificial Neural Network, *Journal of Mechanical Engineering*, Vol. ME 40, Issue 2, Dec 2009, pp. 119-130.

[16] YassineElyassami, KhalidBenjelloun and Mohamed El Aroussi (2016), Bearing Fault Diagnosis and Classification Based on KDA and Alpha-Stable Fusion, *Journal of Contemporary engineering Sciences*, Vol. 9, Issue 10, pp. 453-465.

[17] Yusuf Kayal, IIsmail Ucun and Kubilay Aslantaş (2009), Contact fatigue failure of a tapered roller bearing used in a lorry wheel, *Journal of Failure Analysis and Prevention*, Vol. 9, Jun 2009, pp. 288-294.

[18] Zhihai Wang, Xing Wua, Xiaoqin Liu, Yongli Cao, Jinkui Xie (2017) **,** Research on feature extraction algorithm of rolling bearing fatigue evolution stage based on acoustic emission, *Mechanical systems and signal processing*, Vol 113, July 2017, pp. 271-284

[19] Hosseini Sadegh, Ahmadi Najafabadi Mehdi, Akhlaghi Mehdi (2015), Classification of acoustic emission signals generated from journal bearing at different lubrication conditions based on wavelet analysis in combination with artificial neural network and genetic algorithm, Journal of Tribology International, Vol. 95, November 2015, pp. 426-436